



119
923
THS



This is to certify that the
thesis entitled
**STUDIES OF QUENCHED DIFFUSION FLAMES
NEAR COLD, INERT SURFACES**

presented by

NANDA KISHORE LAKKARAJU

has been accepted towards fulfillment
of the requirements for

M.S. degree in Mechanical Engineering

Dr. Indrek S. Wichman

Major professor

Date January 8, 1996

**LIBRARY
Michigan State
University**

**PLACE IN RETURN BOX to remove this checkout from your record.
TO AVOID FINES return on or before date due.**

DATE DUE	DATE DUE	DATE DUE
_____	_____	_____
_____	_____	_____
_____	_____	_____
_____	_____	_____
_____	_____	_____
_____	_____	_____
_____	_____	_____

**STUDIES OF QUENCHED DIFFUSION FLAMES
NEAR COLD, INERT SURFACES**

By

NANDA KISHORE LAKKARAJU

A THESIS

**Submitted to
Michigan State University
in partial fulfillment of the requirements
for the degree of**

MASTER OF SCIENCE

Department of Mechanical Engineering

1996

ABSTRACT

STUDIES OF QUENCHED DIFFUSION FLAMES NEAR COLD, INERT SURFACES

By

Nanda Kishore Lakkaraju

This project deals with the study of quenched diffusion flames near cold, inert surfaces. It examines the structure of the flame-tip region of a triple or a tribrachial flame. A transformation of coordinates is employed that enables the energy equation to be integrated across the pre-mixed flame arc, subject to an upstream matching condition. An approximate matching condition is derived that enables an equation for the PF arc shape. The solution of this equation produces flame shape contours $X(Z)$ which may then be grafted onto an orthogonal grid employing flame coordinates, $\chi-Z$; that is, the flame shape is described by an equation of the type $\chi = X(Z)$. A comparison is made between the shapes calculated using this simplified theory and numerically computed flame shapes; it was found to be favorable. Weaknesses of this analysis are discussed, and possibilities for future work are examined.

ACKNOWLEDGEMENTS

I wish to thank my major professor Dr. Indrek S. Wichman without whose guidance this project would not have come out in this manner. I would also like to thank Dr. Bassem Ramadan and Mr. Anjan Ray whose work was used for a part of this project.

I also wish to acknowledge the support of Dr. Vedha Nayagam and Dr. Milton Linevsky, who were the contract monitors for this project at NASA μ g Combustion Research and NSF Thermal Sciences Division respectively.

I would also like to acknowledge the guidance of my parents who are primarily responsible in my pursuing graduate study.

TABLE OF CONTENTS

	LIST OF FIGURES	(v)
	NOMENCLATURE	(vi)
	PREAMBLE	1
	INTRODUCTION	5
Chapter 1	THE INNER PROBLEM	11
Chapter 2	THE OUTER PROBLEM	20
Chapter 3	Z-FIELD CALCULATION	26
Chapter 4	RESULTS AND DISCUSSION	32
Chapter 5	CONCLUSIONS & RECOMMENDATIONS	
	FOR FUTURE WORK	51
	BIBLIOGRAPHY	53

LIST OF FIGURES

		<u>Page No</u>
Fig 1.	Some representative triple flame problems	7
Fig 2.	The outer problem, and its solution showing the orthogonal system of coordinates	10
Fig 3.	The physical configuration, including the laboratory coordinates(x,y), the mass flow, ϵ , the PF arcs, and the trailing downstream DF .	12
Fig 4.	Diagram of the (a) actual temperature distribution (t) and (b) stretched temperature ($\theta=\beta(1-\tau)$) distribution across a typical PF	19
Fig 5.	A hypothetical triple flame structure.	21
Fig 6.	Plots showing reorientation of the coordinate system.	27
Fig 7.	Sample test plot of the PF arcs.	35
Figs. 8-19	Premixed flame arcs superposed onto the orthogonal coordinate system. The reactivity contours are also plotted for the same case.	36-47
Fig 20.	Grid system for different epsilon values.	48
Fig 21.	Plot of dZ/dY for the domain.	49
Fig 22.	Plot of dZ/dX for the domain.	50

NOMENCLATURE

b	Asymptotic parameter
c	“wave speed”
D	Damköhler number
\hat{E}	Activation energy
f	Upstream matching function $f = -\tau_\eta$,
H	Excess enthalpy function
R	Universal gas constant
r_q	Quench radius
s	PF arc slope, $s = dx/dy$
\hat{t}	Dimensional temperature
\hat{t}_0	Dimensional ambient temperature
$\hat{t}_0(Z)$	Outer (dimensional) temperature profile
T_f	Adiabatic flame temperature
x	Physical coordinate (non dimensional)‘
X	PF arc coordinate
X_0	Furthest upstream PF point
y	Physical coordinate (non dimensional)
Z	Mixture fraction, $Z = (\phi y_F + 1 - y_0)/(1 + \phi)$

^
:
:
Q
O
X
V
W

^
DF
PF
TP
AE

GREEK

β	Non dimensional activation energy
γ	Function containing $\text{abs}(Z-Z_f)$
ε	Convective flow parameter
η	Non dimensional coordinate
θ	Stretched temperature
κ	Temperature gradient parameter
Λ	Eigenvalue relationship
ξ	Non dimensional coordinate
τ	Non dimensional temperature
Φ	Flame shape function
ϕ	Global stoichiometric coefficient
χ	Coordinate grid orthogonal to Z
ψ	$\psi=Z-1/2$
ω	Reaction rate function

SUPERSCRIPTS, SUBSCRIPTS and ABBREVIATIONS

\wedge	Dimensional quantity
DF	Diffusion flame
PF	Premixed flame
TP	Triple point
AEA	Activation-energy asymptotics

ton
qu
ing
me
to t
flar
tors
but
con
it av
plica
circu
need
with
struct

PREAMBLE

The **triple-flame structure** is important for flame attachment in combustors with fuel injectors. Without a certain degree of premixing these flames would either quench or blow off. The same is true to a less dramatic extent for flame attachment involving flame spread over liquid or solid fuels. Here the flow comes from the condensed medium, which is gasifying, whereas the oxidizer flow originates upstream and is parallel to the pyrolyzing surface. Once again, a mixing region is formed that largely controls the flame spread dynamics. This mixing region has been noted by even the earliest investigators, both experimental and numerical (and, in principle, the theoretical investigators, too) but fundamental examinations of the nature and detailed structure of this zone were not conducted. Part of the reason is the smallness of the region, it being convenient to “assume it away” by a boundary layer approximation, for example. Another difficulty is the complicated nature of the interacting processes, most of which are not “visible” under ordinary circumstances but require extreme limits in order to bring them into bold relief. What is needed, therefore, is a detailed examination of a model problem concerned directly not with flame spread or flame attachment or any other practical feature but with the flame structure itself.

inject

meabi

overall

diffus

of the

mixed

toward

the sec

eral id

sity. T

densit

release

cesses

ing ox

fractio

occur t

exagger

The model problem examined here describes qualitatively either a fuel injector-type problem or a flame spread problem. The fuel flows past one side of an impermeable divider and mixes with an oxidant that flows past its other side. Depending on the overall stoichiometry, as measured through the overall stoichiometric index, the resulting diffusion flame (**DF**) inclines either to the left or to the right of the divider. On either side of the **DF** and originating at its furthest upstream point (the triple point, **TP**) are two premixed flames (**PFs**), one projecting toward the oxidizer side (lean **PF**) and the other toward the fuel side (rich **PF**). The resultant structure, the triple (or tribrachial) flame, has the seemingly curious ability to propagate faster than the completely premixed flame. Several idealizations are made in this study.

The first idealization is that the flow field is inviscid and has constant density. This effectively eliminates the flame acceleration effect which is primarily a variable-density phenomenon coupled with the occurrence of extremely high rates of reaction (heat release) near the **TP**. Prior to entering into detailed discussions of coupled physical processes, we examine why the reaction rate near **TP** becomes as large as it does by calculating oxidizer, fuel and temperature profiles there. Qualitatively, the oxidizer and fuel fractions are both non-negligible but the temperature is quite close to its maximum value.

The second idealization is for the chemical reaction which is assumed to occur through a single irreversible step $F + \nu O \rightarrow (1+\nu) P$. This, we know, highlights or exaggerates the triple flame structure, but for a modeling study it is exactly what we need.

R

li

re

so

ins

bee

and

exam

quen

minor

oated

specie

shed n

is curr

flux sig

liquid f

changes

Reasonably useful one-step schemes for $\text{CH}_4\text{-O}_2$ exist which may be used to assess the likely regions of parameter space occupied by actual HC reaction schemes. More realistic reaction schemes (e.g., $\text{H}_2\text{-O}_2$) may be examined later.

The third idealization is unity Lewis numbers for both fuel and oxidizer. In some cases the Lewis number may become small enough to promote extreme forms of instability, but this complication is best left for future work once preliminary details have been sorted.

The objective of this work is to develop a means for combining numerics and asymptotics so that a detailed diagnosis of the flame structure can be made. A recent example of such a method is given in the article of Wichman and Bruneaux [1996], on the quenching of a premixed flame by a cold wall. Inflection points, local maxima and local minima were all interpreted physically, resulting in a clearer understanding of this complicated process. We believe that the examination of the excess enthalpy function H , and the species y_0, y_f , and temperature, τ , profiles and their various derivatives and gradients will shed much light on the triple flame structure. The numerical/asymptotic solution method is currently being developed and implemented for zero-convection flames.

A practical objective of future research is the examination of flame heat flux signatures. These heat flux signatures play a major role in flame spread over solid and liquid fuels. We expect that significant variations of the heat fluxes are produced by changes in chemical parameters like the Damköhler number, D , the activation energy, β ,

the flow

these in

tance as

tion cas

indicatir

over sol

really ex

and the I

from the

supply. F

modeling

numerics

these asy

the flow rate, ϵ , and the overall stoichiometry (ϕ). The challenge here will be to quantify these influences and to devise correlations for engineering use, if possible.

Another practical objective is the examination of the flame quenching distance as a function of D , β , ϵ , ϕ . A useful correlation formula exists for the zero convection case, $\epsilon=0$. An interesting goal here is to produce a “map of parameter space” indicating what sorts of triple flames exist in each region. For instance, for flame spread over solid fuels we find that the **PF** arc closest to the fuel surface (the rich **PF**) does not really exist, so the triple flame reduces to a double flame composed of only the lean **PF** and the **DF** arc. For flame spread over liquids, however, the flame structure is lifted further from the surface because the pre-existing liquid vapor enable burning further from the fuel supply. Hence the classical three-branch triple flame is observed.

The goals of this study, however, are to explore the limits of simplified modeling in the description of a complex problem. If the asymptotic approach and the numerics are in reasonable agreement, we shall be more confident in our goal of extending these asymptotic and other analytically-based ideas to the more general problem.

fusi

pre

a.ri

fla:

bet

In

ena

fiel

"eq

indi

proy

inba

INTRODUCTION

The triple flame (or tribrachial flame) is usually found near the tip of a diffusion flame (**DF**). On one side, the unburned fuel mixes with the oxidizer to form a lean premixed flame (**PF**). On the other side, the unburned oxidizer mixes with the fuel to form a rich **PF**. The resultant structure, **DF** with the attached **PFs**, is called a triple or tribrachial flame.

Triple flames are generally found in regions where there is a transition between low Damköhler number mixing and high Damköhler number diffusional burning. In the regions where the Damköhler number is small, the chemical reaction is “*frozen*”, enabling unrestricted mixing to occur between the fuel and the oxidant. In a general flow field, these regions will be separated from zones of large Damköhler number, called “*equilibrium*” regions, where it is impossible for the fuel and the oxidizer to coexist.

There is one dominant feature of the triple flame that makes it indispensable in practical combustion systems. It enables the **DF** - guided by two **PFs** - to propagate into, or against, an opposing flow. This explains how **DFs**, which have no inherent propagation velocity, can survive in regions of relatively high flow velocities. A

few repr

opposed

combust

triple flu

ing regio

ing zone

beginnin

ignoring

deRis, a

can des

pyrolyz

the flamm

be perf

thesized

structure

initially

few representative triple flame problems (see Fig. 1) are (a) "bunsen flame" attachment, (b) opposed-flow flame spread, (c) wind-aided flame spread, (d) jet diffusion flames, (e) combustors, (f) flame propagation in stratified mixtures etc. In each of these problems, the triple flame problem arises as an important sub-problem.

In opposed-flow flame spread, for example, there must be a flame anchoring region that allows the DF to survive the opposing flow of the oxidizer. Thus, a premixing zone of low Damköhler number must exist near the flame tip. An approximate, or beginning understanding of the nature of this flame spread problem can be gained by ignoring the triple flame region entirely, leading to the standard heat transfer models of deRis, and Wichman and Williams. However, if sophisticated models are sought which can describe the influences of finite-rate reaction, detailed heat flux signatures* to the pyrolyzing fuel, and detailed solid-phase decomposition, then, the triple flame structure in the flame tip region must be examined

Since the full problem is difficult to solve, the triple flame calculation must be performed separately as a subproblem. *It is a part of the whole that must later be synthesized into the complete solution.*

This project attempts to examine the fundamental nature of the triple flame structure. A "two stream" problem is considered, where the fuel and oxidizer streams are initially separated by an inert divider. This problem is then divided into two subproblems:

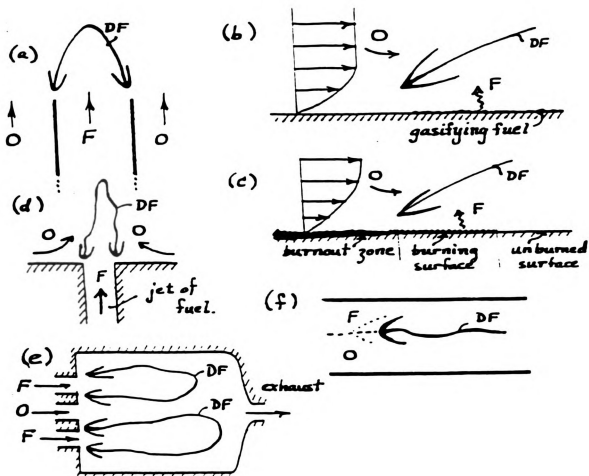


Fig 1. Some representative triple flame problems

(a)

↑
0

(d)

—
—

(e)

F-

0-

F.

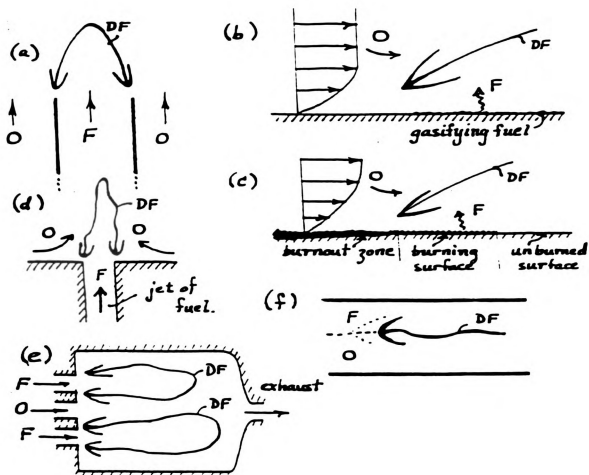


Fig 1. Some representative triple flame problems

an inner

near the

occurs. The

PFs and t

the inner

dinate. Z

is rather

nates are

makes th

less, the

ever can

examine

boundar

beforeha

at unkno

numeric

this repo

limiting

distribut

an inner problem and an outer problem. The physical domain for the outer problem is near the quenching zone between the inert divider and the point at which extinction occurs. The inner problem is solved relatively close to the point of attachment of the two **PFs** and the trailing **DF**.

The solution to this problem is achieved in three stages. In the first stage, the inner problem is solved in order to obtain a relation between the mixture fraction coordinate, **Z**, and the flame coordinate, **X**. Generally, the inner problem in combustion theory is rather straight-forward once the scalings are determined and the relevant inner coordinates are known. The dominant variation occurs across the flame width, not along it. This makes the mathematical problem one-dimensional, though generally nonlinear. Nevertheless, the inner problem is usually well posed and rather easily solved.

In the second stage, the outer problem is tackled. The outer problem, however can be much more difficult, especially in multi-dimensional geometries like those examined here. The principal difficulty involves the precise location of the matching boundary. This unknown quantity must derive from the solution; it is generally not known beforehand. Hence, the outer problem is solved subject to unknown boundary conditions at unknown segments of the boundary making it an ill-defined Cauchy problem. Clearly, numerical methods of solution will be necessary, the general procedure being iterative. In this report, we examine an exact representation of the out solution. A logically reasonable limiting case of this general expression produces a simplified outer temperature-gradient distribution that can be comfortably matched to the inner solution. Although, thorough

math

has to

ortho

mixtu

solvim

solutio

a reali

of the

compar

obtaine

bounda

etc., are

2.b. Un

(β, D), th

duce as

with an

be encou

mathematical rigor is absent, a satisfactory self-consistency is nevertheless obtained.

In the third stage, the solution for the inner problem, obtained in stage one, has to be grafted onto the solution obtained in stage two. In order to achieve this, first an orthogonal coordinate system must be developed, one of the coordinates of which are the mixture fraction coordinate contours. An orthogonal set of contours χ - Z , is obtained by solving the appropriate differential equation governing the field. Once this is obtained, the solutions for the **PF** arcs, $\chi = X(Z)$, can be grafted onto this coordinate system which gives a realistic picture of the triple flame arcs as oriented in space.

In this report, the reactivity contours computed from a numerical solution of the full equations are superposed on our solution for the **PF** arcs. This can be a useful comparison in validating the results obtained from this simplified theory and those obtained from exact numerical calculations. The numerical solutions are generated for the boundary-value problem illustrated in Fig. 2.a, where the equations, boundary conditions, etc., are shown. The reactivity contours, which are lines of constant ω , are plotted in Fig 2.b. Under many flow conditions (ϵ), with a fairly wide range of chemical parameters (β, D), the characteristic triple flame shape is obtained. Our goal in this report is to reproduce as closely as possible the skeletal features of these numerically-calculated results with an asymptotic flame theory. If a reasonable level of agreement is obtained, we shall be encouraged to move to the next level of sophistication in our calculations.

7.

2.5

2

1.5

0.5

The fundame

equations an

in the negativ

phase proper

flame chemis

mass fraction

The fuel and

coefficient H

$\phi = Y_{FF} Y_{OO}$

ive flow $\epsilon = 0$

Property ener

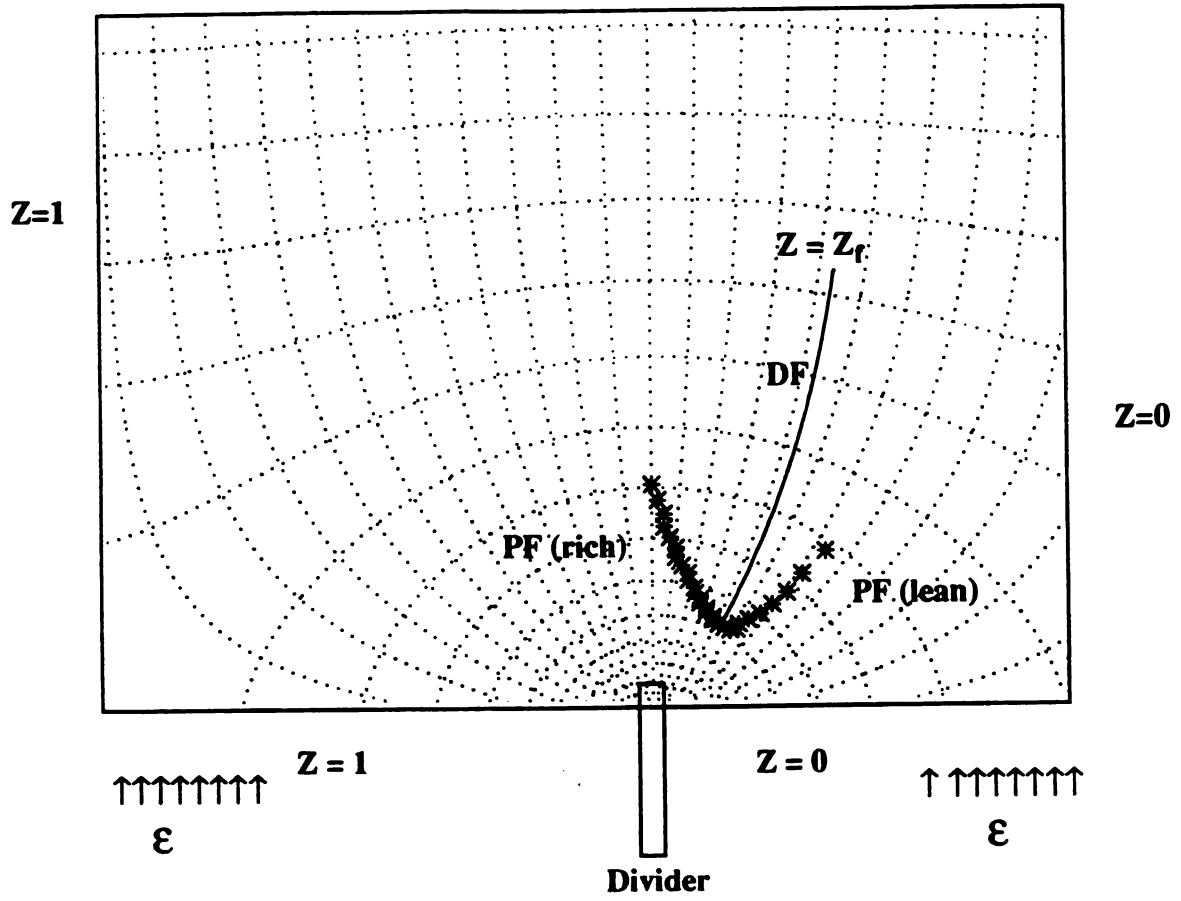
CHAPTER 1

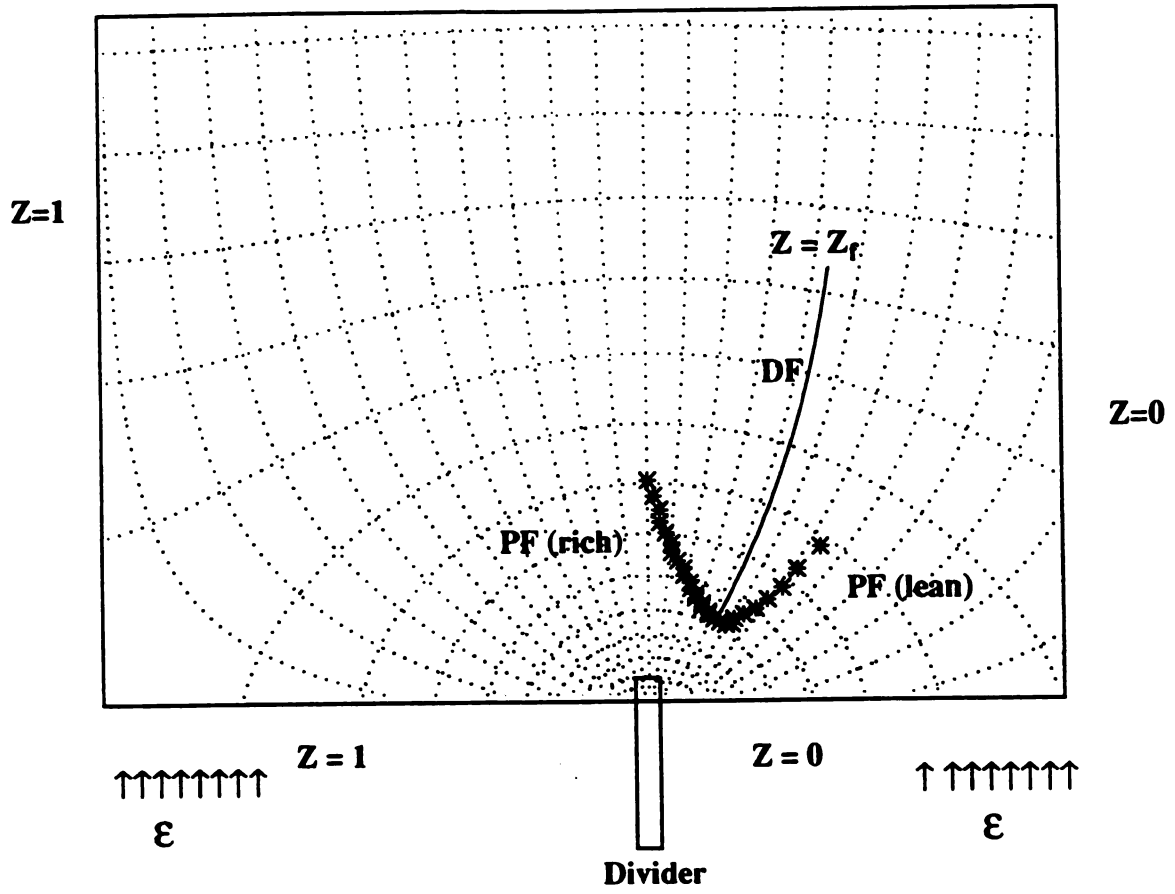
THE INNER PROBLEM

In our simplified model, the inner zone that we shall examine is the PF arc. The fundamental boundary value problem is illustrated in Fig. 2.a; these are the basic equations and boundary conditions that we shall study. The flow past the vertical divider in the negative- x half-plane is inviscid and incompressible (i.e., constant density). The gas phase properties are assumed constant and a one step irreversible reaction describes the flame chemistry. The diffusion coefficients of fuel and oxidizer are assumed identical, the mass fractions are $y_F = Y_F/Y_{FF}$ and $y_O = Y_O/Y_{OO}$, which vary between zero and unity. The fuel and oxidizer equations can be combined to produce a homogeneous constant-coefficient Helmholtz equation for the mixture fraction $Z = (\phi y_F + 1 - y_O)/(1 + \phi)$, where $\phi = \nu Y_{FF}/Y_{OO}$ is the overall or global stoichiometric coefficient. In the case of zero convective flow $\epsilon=0$, it is easy to solve for Z and to obtain:

$$Z = \frac{1}{\pi} \cdot \operatorname{atan} \left(\frac{\tan \left(\pi \frac{y}{2} \right)}{\tan h \left(\pi \frac{x}{2} \right)} \right). \quad (1)$$

For the triple flame problem shown in Figs. 2 and 3, we write the constant property energy equation here as





$$\varepsilon \tau_x = \tau_{xx} + \tau_{yy} + (1 + \phi) D\omega, \quad (2)$$

which we transform into the ξ - η plane near the PF (see Fig. 3). The coordinates (x,y) span the complex z -plane, $z = x + iy$, and the coordinates (ξ,η) span the complex w -plane, $w = \xi + i\eta$. Coordinate ξ follows the **PF** sheet, which we have defined as the locus of points $\eta = 0$. Also, $\eta = \xi = 0$ at the triple point, **TP**. Note that the coordinate η increases in the downstream direction.

Mathematically, we write

$$z = x + iy = f(\xi + i\eta) = f(w),$$

$$w = \xi + i\eta = g(x + iy) = g(z).$$

Note that the **PF** arc should be piecewise continuous. This means slope discontinuities are permitted, so that **PF** arc shapes of the kind discussed previously are allowed.

An improved understanding of the relationship between the flame structure and the cartesian system (x,y) is obtained when we press the analysis further. First, we define the flame locus as $x = X(y)$. The local flame slope is $s = dX(y)/dy = s(y)$. We wish to develop the function $f(w)$ such that along the flame locus, there is a one-to-one correspondence between ξ and y . That is, along the flame locus we require

$$Z = X(y) + iy = f(\xi) = X(\xi) + i\xi.$$

Hence, along the flame arc, where $y = \xi$, we have $s(y) = f'(\xi)$. Consequently,

$$f'(\xi) = s(\xi) + i, f''(\xi) = s'(\xi), f'''(\xi) = s''(\xi), \text{ etc.}$$

For small η

Now we show

$$y(\xi, \eta)$$

x

from the x-y

line

When $\Delta z =$

and for $\Delta z =$

g

For small η , we can write the Taylor expansion for $f'(\xi+i\eta)$ as

$$\begin{aligned} f'(\xi+i\eta) &= f'(\xi) + (i\eta)f''(\xi) - (\eta^2/2!)f'''(\xi) + \dots \\ &= (s - (\eta^2/2!)s'' + \dots) + i(1 + \eta s' + \dots) = \mu + i\lambda. \end{aligned}$$

Now we shall examine the function $f(w)$ in order to obtain expressions for $x(\xi, \eta)$ and $y(\xi, \eta)$.

$$\begin{aligned} x + iy &= f(\xi + i\eta) = f(\xi) + i\eta f'(\xi) + i\eta^2/2! f''(\xi) + \dots \\ &= f(\xi) + i[\eta s - \eta^3 s''/3! + \dots] - [\eta + \eta^2 s'/2! + \dots] \\ &= [X(\xi) - (\eta + \eta^2 s'/2! + \dots)] + i[\xi + \eta s - \eta^3 s''/2!]. \end{aligned}$$

We require one more piece of information before we transform our equations from the x - y coordinate system to the ξ - η coordinate system. Given $w = \xi + i\eta$, we calculate

$$\begin{aligned} \frac{d}{dz} [g(z)] &= [g(z_0 + \Delta z) - g(z_0)] / (\Delta z) . \\ &= \{\xi(x_0 + \Delta x, y_0 + \Delta y) - \xi(x_0, y_0) + i[(x_0 + \Delta x, y_0 + \Delta y) - \eta(x_0, y_0)]\} / (\Delta x + i\Delta y). \end{aligned}$$

When $\Delta z = \Delta x$, we obtain

$$g'(z_0) = \xi_x(x_0, y_0) + i\eta_x(x_0, y_0)$$

and for $\Delta z = i\Delta y$, we obtain

$$g'(z_0) = \eta_y(x_0, y_0) - i\xi_y(x_0, y_0).$$

This leads dire

$\xi =$

$\eta_x =$

Hence.

$\frac{\partial}{\partial x}$

$\frac{\partial}{\partial y}$

so that the La

∂

Substitution

We observe

Hence.

giving fr

This leads directly to the Cauchy-Riemann conditions,

$$\xi_x = \eta_y,$$

$$\eta_x = -\xi_y.$$

Hence,

$$\frac{\partial}{\partial x} = \xi_x \partial_\xi + \eta_x \partial_\eta = \xi_x \partial_\xi - \xi_y \partial_\eta,$$

$$\frac{\partial}{\partial y} = \xi_y \partial_\xi + \xi_x \partial_\eta,$$

so that the Laplacian operator transforms as

$$\partial_{xx} + \partial_{yy} = \left(\xi_x^2 + \xi_y^2 \right) (\partial_{\xi\xi} + \partial_{\eta\eta}).$$

Substitution into the energy equation (2) gives

$$\left(\frac{\xi_x}{\xi_x^2 + \xi_y^2} \right) \cdot \tau_\xi = \left(\frac{\xi_y}{\xi_x^2 + \xi_y^2} \right) \tau_\eta + \tau_{\eta\eta} + \tau_{\xi\xi} + \frac{(1 + \phi) D\omega}{\left(\xi_x^2 + \xi_y^2 \right)}. \quad (3)$$

We observe that $\xi_x = \text{Re}(g')$, $\xi_y = -\text{Im}(g')$, and that

$$\frac{df}{dw} = \frac{dg^{-1}}{dz} = \mu + i\lambda.$$

Hence,

$$\xi_x = \mu(\mu^2 + \lambda^2), \quad \xi_y = \lambda(\mu^2 + \lambda^2), \quad \xi_x^2 + \xi_y^2 = (\mu^2 + \lambda^2)^{-1},$$

giving, from (3)

$$\varepsilon \mu \tau_x = \varepsilon \lambda \tau_\eta + \tau_{\eta\eta} + \tau_{\xi\xi} + \left(\mu^2 + \lambda^2 \right) (1 + \phi) D\omega. \quad (4)$$

This equation can be analyzed across the **PF** arc (across which only η varies). Across the **DF**, we see that only ξ varies once the arc ξ has specified. Consequently, equation (2) may be analyzed along the **PF** arc by stretching eta, along the **DF** by stretching ξ . Near the **TP**, both ξ and η must generally be stretched so that equation (4) remains elliptic there¹.

At the **PF**, we define $N = b\beta\tau$ as the stretched coordinate normal to the PF arc.

Hence, (4) becomes,

$$\tau_{NN} = \frac{\left(-(\mu^2 + \lambda^2)\right)(1 + \phi) D\omega}{b^2\beta^2} + \frac{[\epsilon\mu\tau_\delta - \epsilon b\beta\lambda\tau_N - \tau_{\xi\xi}]}{b^2\beta^2}. \quad (5)$$

As $\beta \rightarrow \infty$, the second term on the RHS vanishes by comparison with the first.

As $\beta \rightarrow \infty$, the factor $\mu^2 + \lambda^2$ is evaluated along the **PF**. We recall that

$$x + iy = f(\xi + i\eta) \text{ and that}$$

$$f'(\xi) = \mu + i\lambda = s(\xi) + i,$$

where s is the local flame slope. Hence, $\mu^2 + \lambda^2 = \text{abs}(f'(\xi))^2 = 1 + s^2$, giving

1. *Presently, we must note the usefulness of a transformation to a system of coordinates employing Z as the coordinate perpendicular to the **DF** locus. The work of Peters and Bilger and others is predicated upon the usefulness of this transformation. However, it is quite obvious that for more complicated flame structures like triple flames, the "natural" ξ - η coordinate system is far more appropriate*

$$\tau_{NN} = \frac{-(1+s^2)(1+\phi)D\omega}{b^2\beta^2}, \quad (6)$$

where the reaction rate function is given by

$$\omega = y_0 y_f \exp[-\beta(1-\tau)/[1-\alpha(1-\tau)]],$$

with

$$y_0 = 1 - Z - (1 - Z_f)\tau,$$

$$y_f = Z - Z_f\tau.$$

We now perform a standard high Activation Energy Asymptotic (AEA) analysis, (Linan (1974)) letting

$$\tau = \tau_0(z) - \theta/\beta b$$

with

$$\theta = \theta_0 + \theta_1/\beta + \dots$$

and

$$b = [1 - \alpha(1 - \tau_0(z))] = \left[\frac{\hat{T}_f}{\hat{T}_0} \right]^2.$$

After a little algebra (recall that $Z_f = 1/(1+\phi)$) we find that for the fuel side ($Z > Z_f$)

$$\tau_{NN} = \left[\frac{\left(-\left(1 + s^2 \right) \right) (1 - Z_f) \exp \left(\frac{\hat{E}}{\hat{R}} \cdot \left(\frac{1}{T_f} - \frac{1}{\hat{T}_o(z)} \right) \right)}{b^4 \beta^4} \right] \theta (\theta + \gamma_f) \exp(-\theta_0) \quad (7)$$

and for the oxidizer side ($Z < Z_f$)

$$\tau_{NN} = \left[\frac{-\left(1 + s^2\right) \cdot (1 - Z_f) \exp\left(\frac{\hat{E}}{\hat{R}} \cdot \left(\frac{1}{T_f} - \frac{1}{\hat{T}_o(z)}\right)\right)}{b^4 \beta^4} \right] \theta (\theta + \gamma_o) \exp(-\theta), \quad (8)$$

where $\gamma_f = \beta b(Z - Z_f) / Z_f[(1 - Z_f)]$ and $\gamma_o = \beta b(Z_f - Z) / Z_f[(1 - Z_f)]$. We now note that

$$\theta_{NN} = \frac{\partial^2}{\partial N^2} \left[\tau_0(Z) - \frac{\theta}{\beta b} \right] = \tau_0(Z)_{ZZ} \left(\frac{\partial Z}{\partial N} \right)^2 - \frac{\theta_{NN}}{\beta b} = -\frac{\theta_{NN}}{\beta b} \quad (9)$$

because $\tau_0(Z)$ is a linear function of Z and its second derivative always vanishes (except at $Z = Z_f$). Hence, we can write the previous two equations under a single notation:

$$\theta_{NN} = \Lambda(Z) \cdot \theta (\theta + \gamma(z)) \exp(-\theta), \quad (10)$$

with boundary conditions $\theta_N \rightarrow 0, \theta \rightarrow 0$ as $N \rightarrow \infty$ (burnt side) and $\theta_N \rightarrow f, \theta \rightarrow \infty$ as $N \rightarrow -\infty$ (unburned side). Integration of these equation provides the following eigen-relationship.

$$\Lambda(z) = \frac{f^2}{2(2 + \gamma)}, \quad (11)$$

where

$$\Lambda(z) = \frac{\left(-\left(1 + s^2\right)\right) (1 - Z_f) D(Z)}{b^3 \cdot \beta^3}, \quad (12)$$

$$\gamma_f = \beta b(Z - Z_f) / Z_f[(1 - Z_f)],$$

$$b = [1 - \alpha(1 - \tau_0(Z))] = \left[\frac{\hat{T}_f}{\hat{T}_0} \right]^2.$$

In order to determine the flame shape from the solution for s , the function “ f ”

must be known. Function “f” connects the inner PF-zone solution to the upstream quench zone. From our inner/outer transformation, it is easily shown that $f = \theta_N = -\tau_\eta$. Since τ increases with increase of η in front of the PF arc, (i.e., $\tau_\eta > 0$) we expect $f < 0$ there. See Fig 4 below:

Fig 4 below:

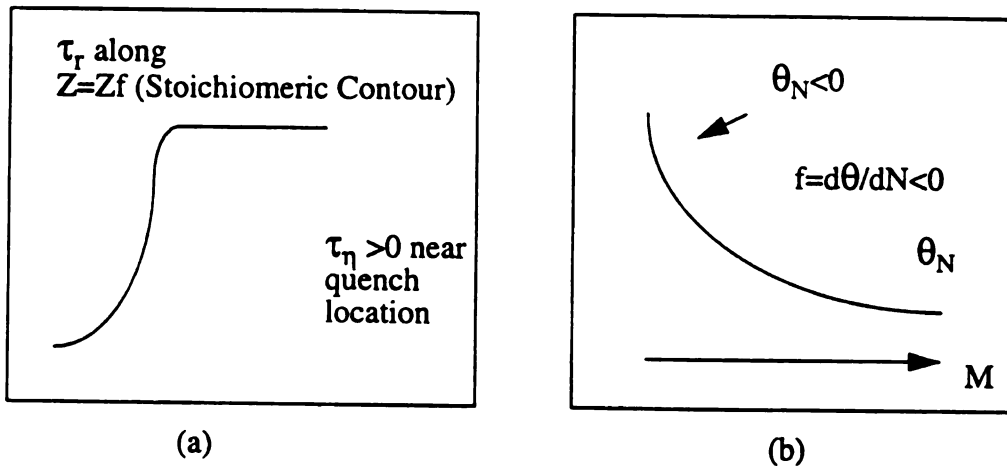


Fig 4. Diagram of the (a) actual temperature distribution (τ) and (b) stretched temperature ($\theta = \beta(1 - \tau)$) distribution across a typical PF

The novel feature of our premixed flame analysis at this stage is the initial transformation to the flame coordinate system. What remains of this transformation after integrating and matching is the local flame slope, s , which is presently unknown. The subsequent analysis of the following sections is constructed in such a manner that the function, s can be determined.

CHAPTER 2

THE OUTER PROBLEM

We observe generally that the outer upstream solution has a rather strong bearing on the calculated results. In Dold's formulation (1989), the parameter ε (containing the flame speed) plays a prominent role. Nevertheless, the outer solution was little more than a transversely slowly varying pre-mixed flame, in a semi-infinite medium. Hence, Dold's model (1989) was a minor perturbation from the standard free **PF** outer solution. Other outer solutions are clearly possible under different conditions of flame attachment.

The solution that we shall develop is exact though fundamentally without use until certain rational and self-consistent simplifications are made. We note that it is typically the outer problem that is the most difficult to solve, and that only in certain special cases (e.g., the 1-D steady **PF**) is the outer solution easily found. The chief difficulty in this triple-flame calculation resides precisely in the outer problem we now examine.

Evaluation of τ_{η} at the PF:

Let us consider a fairly general formulation shown in Fig. 5. Here 'x' is the streamwise coordinate (in the direction of the prevailing flow) and 'y' is the transverse coordinate.

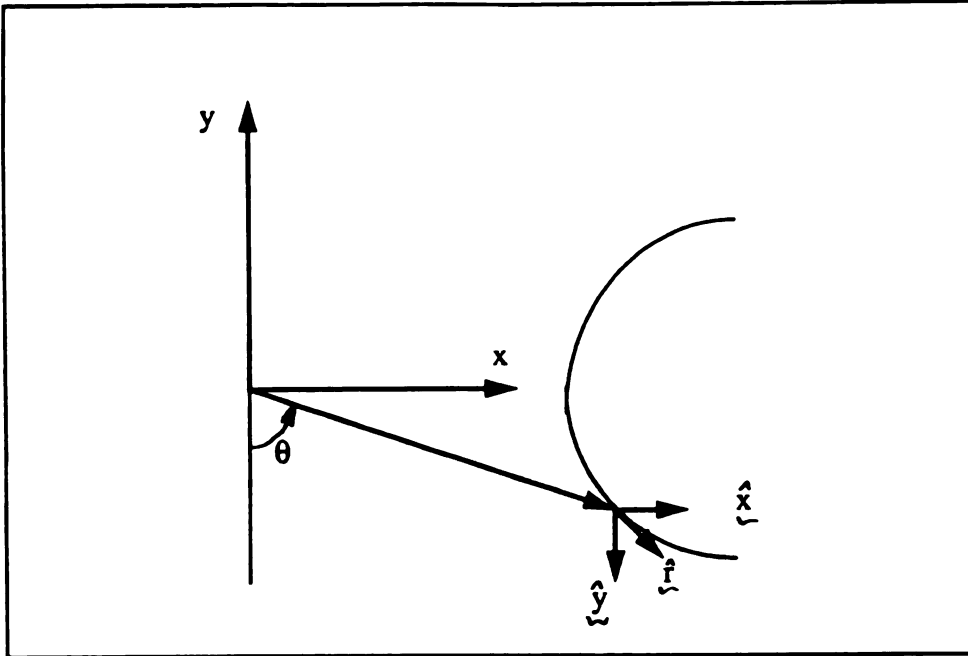


Figure 5. A Hypothetical Triple Flame Structure

We write the general formula,

$$\tau_{\eta} = \nabla \tau \cdot \hat{\eta}. \quad (1)$$

In polar coordinates this becomes,

$$\nabla \tau = \hat{r} \tau_r + \left(\frac{\hat{\theta}}{r} \right) \tau_{\theta}. \quad (2)$$

The **PF** arc is given by $x = X(y)$ or $F = x - X(y) = 0$. Clearly $F > 0$ on the burnt side and $F < 0$ on the unburned side. For this reason, we define the unit vector in the η -direction (positive in the direction $F > 0$) as

$$\hat{\eta} = \frac{\hat{\nabla} f}{|\hat{\nabla} f|}$$

Hence

$$\tau_\eta = \nabla \tau \cdot \hat{\eta}$$

becomes

$$\tau_\eta = \frac{\tau_r (\sin \theta + s \cos \theta)}{\sqrt{(1+s^2)}} + \frac{\tau_\theta (\cos \theta - s \sin \theta)}{\sqrt{(1+s^2)}},$$

where we have used $\hat{x} = \hat{x} \sin \theta - \hat{y} \cos \theta$, $\hat{y} = \hat{x} \cos \theta + \hat{y} \sin \theta$

and the functions, r , $\sin \theta$, $\cos \theta$ can be expressed in terms of y_f and $X(y_f)$ as

$$r = \sqrt{(X + X_0)^2 + y_f^2},$$

$$\sin \theta = \frac{X + X_0}{\sqrt{(X + X_0)^2 + y_f^2}},$$

$$\cos \theta = \frac{-y_f}{\sqrt{(X + X_0)^2 + y_f^2}},$$

where coordinate y_f tracks the **PF** as shown in the previous figure. Therefore

$$\tau_\eta = \frac{1}{\sqrt{(1+s^2)}} \frac{1}{\sqrt{(X + X_0)^2 + y_f^2}} \left\{ \tau_r ((X + X_0) - s y_f) - \tau_\theta \left(\frac{y_f + s(X + X_0)}{\sqrt{(X + X_0)^2 + y_f^2}} \right) \right\}. \quad (3)$$

We note that X_0 is the furthest upstream point on the **PF** locus. When we consider the small limit of X/X_0 , y/X_0 , r/X_0 , then we obtain

$$\tau_\eta \equiv \frac{1}{X_o} \cdot \left(\frac{\tau_r - s\tau_\theta}{\sqrt{(1+s^2)}} \right). \quad (4)$$

The substitution of eqn (4) into eqn (1.11) gives, for the flame slope,

$$s = \pm \sqrt{\frac{1}{\Phi(Z)} - 1}, \quad (5)$$

where

$$\Phi(Z) = \frac{2(1-Z_f)D}{\tau_r^2 \beta^3} \left(1 + \frac{\gamma}{2}\right) \left[\frac{\hat{T}_0(Z)}{\hat{T}_f}\right]^6 \exp\left(\frac{\hat{E}}{\hat{R}} \left(\frac{1}{\hat{T}_o(Z)} - \frac{1}{\hat{T}_f}\right)\right). \quad (6)$$

This result for $\Phi(Z)$ is substituted into the preceding equation for s , enabling us to solve for the flame slope. From the practical point of view the challenge is to determine a suitable approximation for the as-yet-undetermined and unspecified factor τ_r in the upstream vicinity of the **PF** arc.

We realize from previous work and from examination of the two-dimensional outer problem that there are no simple and readily available expressions for τ_r . However, from numerical solutions and purely mathematical considerations, we are relatively confident over the following statements. First, τ_r scales with $1/r_q$, where r_q is the quenching radius. Hence, since the maximum value of τ is unity, we may expect

$$\tau_r \approx \frac{1}{r_q}.$$

Second, τ_r is concave upward toward along the extrapolated **DF** locus in front of the triple point, so that τ_r should actually be greater than $1/r_q$ upstream of the **PF** arc. Consequently,

we can write

$$\tau_r \approx \frac{k}{r_q},$$

with $k > 1$ near to and slightly preceding the **PF** arc, giving

$$\tau_\eta \approx \frac{k}{r_q \sqrt{(1 + s^2)}}. \quad (7)$$

This produces the following expression for $\Phi(Z)$,

$$\Phi(Z) = \frac{2(1 - Z_f) D \cdot r_q^2}{k^2 \beta^3} \left(1 + \frac{\gamma}{2}\right) \left[\frac{\hat{T}_0(Z)}{\hat{T}_f}\right]^6 \exp\left(\frac{\hat{E}}{\hat{R}} \left(\frac{1}{\hat{T}_o(Z)} - \frac{1}{\hat{T}_f}\right)\right), \quad (8)$$

which may be substituted into equation (5) once an outer zone temperature distribution $\hat{T}_0(Z)$ is specified.

There are many possible choices for $\hat{T}_0(Z)$. The detailed nature of the various possibilities will be the subject of a more thorough future mathematical study of eqn (8).

Suffice it to say here that there are two difficulties:

- 1) The maximum value of Φ may not occur at $Z = Z_f$, the DF locus, and
- 2) There is generally a slope discontinuity near $Z = Z_f$, produced by the factor γ .

We have determined that the simplest but perhaps the most unrealistic choice is to use for the oxidizer side of the DF

$$\hat{T}_0(z) = \hat{T}_0 + (\hat{T}_f - \hat{T}_o) \frac{Z}{Z_f} \quad (9)$$

and

$$\hat{T}_0(Z) = \hat{T}_0 + (\hat{T}_f - \hat{T}_o) \frac{(1-Z)}{(1-Z_f)} \quad (10)$$

for the fuel side of the DF.

These formulae for $\hat{T}_0(Z)$ are simply the Burke-Schumann (B-S) temperature profiles. The advantages of the B-S profile are that it produces a maximum for Φ at $Z = Z_f$ which coincides with a manageable slope discontinuity there. From a physical standpoint, this temperature distribution is unrealistic even across the one dimensional downstream DF and we hardly expect it to be realistic in the quenching zone preceding the PF arc. However, for the ease of analysis, it is by far the simplest choice.

To recapitulate, the inner and outer-zone analyses produced the flame slope formula, Eq. (1.11), with the function $\Phi(Z)$ given by Eq. (8), obtained by matching the inner and outer solutions through the condition on τ_η , given originally by Eq. (1.12) and then truncated - for the sake of simplicity- as the Burke-Schumann profile. The PF arc shape is obtained by solving Eq. (5) for the local flame slope, s.

CHAPTER 3

Z-FIELD CALCULATION

In order for the preceding flame slope calculation to be meaningful, a way must be found to relate the flame slope s to the physical coordinates describing the PF locus. Through various transformations, we have produced an equation for s , the local flame slope, in terms of the mass fraction coordinate, Z . The slope itself, however, must be expressed in terms of a coordinate system, (see Fig. 3) that can readily be calculated. In the original rectangular coordinate system, the problem looked as shown below. We have essentially reoriented the coordinate system as shown below (Fig. 6.a), writing $x \rightarrow \tilde{y}$, $y \rightarrow -\tilde{x}$. In the x - y system the transformation from (x,y) to the (u,v) plane shown below (Fig 6.b) is

$$u = \sin \pi \frac{\tilde{x}}{2} \cosh \frac{\pi \tilde{y}}{2}, \quad v = \cos \pi \frac{\tilde{y}}{2} \sinh \frac{\pi \tilde{y}}{2}$$

which in the (x,y) plane becomes

$$u = -\sin \pi \frac{y}{2} \cosh \pi \frac{x}{2}, \quad v = \cos \pi \frac{y}{2} \sinh \pi \frac{x}{2}$$

When $\varepsilon = 0$ (the zero-convection case), the Z equation becomes simply the Laplace equation $\nabla^2 Z = 0$, which also transforms to $\nabla^2 Z = 0$ in the u - v plane. The solution in this

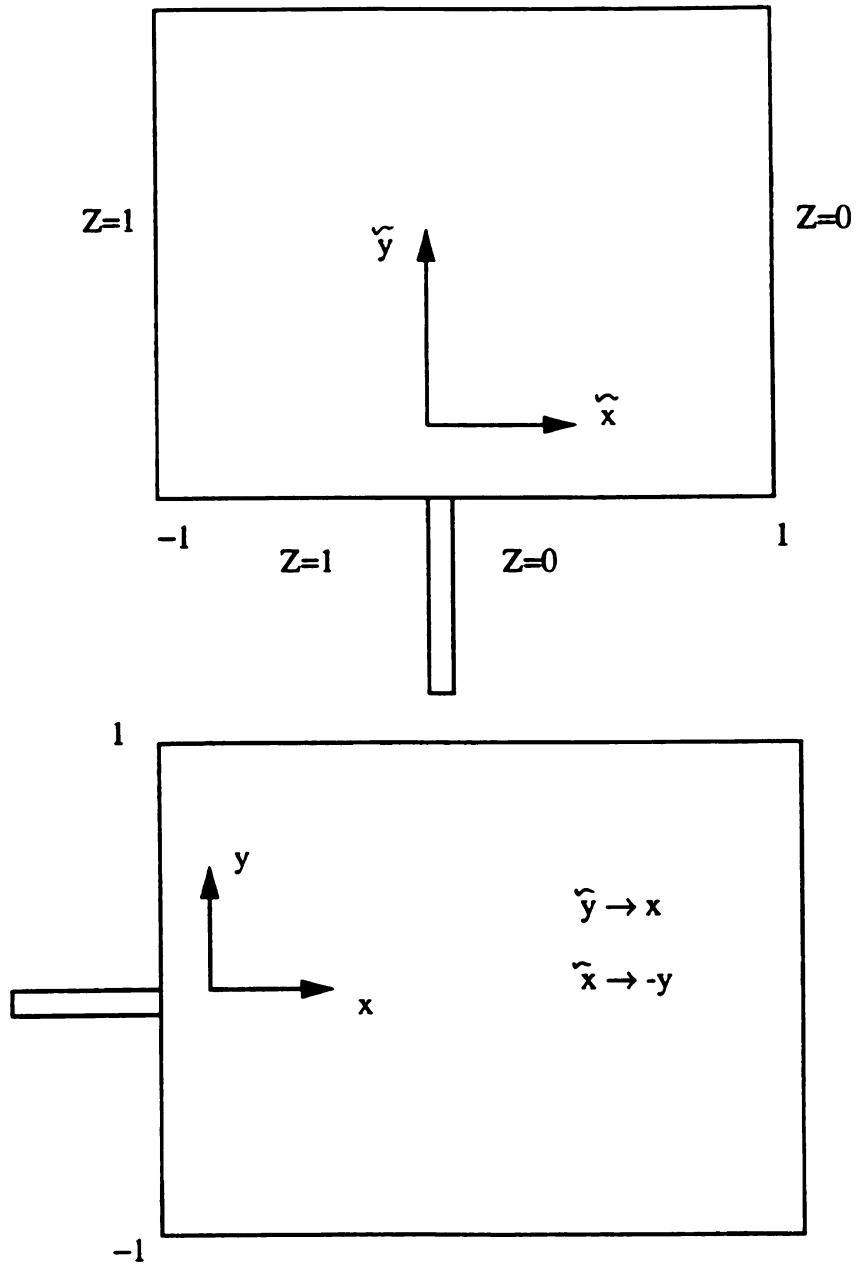


Fig 6. Plots showing reorientation of the coordinate system.

plane, subject to $Z=0$ along the positive u -axis and $Z = 1$ along the negative u -axis, is simply $Z=\theta/\pi$, where

$$\theta = \operatorname{atan}\left(\frac{v}{u}\right) = \frac{1}{\pi} \left[\frac{\pi}{2} + \operatorname{atan}\left(\frac{\tan\left(\pi\frac{\bar{y}}{2}\right)}{\tanh\pi\left(\frac{x}{2}\right)}\right) \right]. \quad (1)$$

The equation for Z is $\varepsilon Z_x = Z_{xx} + Z_{yy}$ subject to $Z=0$ on the oxidizer side and $Z=1$ on the fuel side. In the zero convection case, $\varepsilon=0$, the solution for Z is simply

$$Z = \frac{1}{\pi} \operatorname{atan}\left(\frac{\tanh\pi\frac{x}{2}}{\tan\pi\frac{y}{2}}\right) = \frac{1}{2} + \frac{1}{\pi} \operatorname{atan}\left(\frac{\tan\pi\frac{y}{2}}{\tanh\pi\frac{x}{2}}\right) \equiv Z_0. \quad (2)$$

When $\varepsilon \ll O(1)$, the approximate solution near $Z_0 \approx \frac{1}{2}$, is $Z \approx Z_0 + \varepsilon\left(\theta - \frac{\pi}{2}\right)M + O(\varepsilon^2)$, where $\theta = \pi Z_0$, and M is an $O(1)$ constant that is evaluated numerically from a double integral.

We proceed to calculate dZ/dy for the general case and obtain an expression for dX/dZ in terms of s and dZ/dy . We exploit the fact that $Z=Z(y)$ along the PF arc so that the flame slope can be written as

$$s = \frac{dx}{dy} = \frac{dx}{dZ} \cdot \frac{dZ}{dy} = \frac{dX}{dZ} \cdot \frac{dZ}{dy} \quad (3)$$

Consequently, with dZ/dy given as

$$\begin{aligned}\frac{dZ}{dy} &= \frac{d}{dy} \left[Z_0 + \varepsilon \left(\pi Z_0 - \frac{\pi}{2} \right) M + O(\varepsilon^2) \right] \\ &= (1 + \varepsilon M \pi) dZ_0 / dy,\end{aligned}$$

we calculate $dX/dZ = s / (dZ/dy)$ after passing to the zero flow limit $\varepsilon \rightarrow 0$:

$$\frac{dX}{dZ} = \frac{\left(2\pi \tanh \pi \frac{x}{2} \cdot (\sec \pi \psi)^2 \right) \cdot s}{1 + \left(\tanh \pi \frac{x}{2} \right)^2 \cdot (\tan \pi \psi)^2 - s \left(\operatorname{sech} \pi \frac{x^2}{2} \cdot \tan \pi \psi \right)} \quad (4)$$

where $\psi = Z - 1/2$. This equation can be solved to produce the local flame slope $X(Z)$, once we substitute for ψ, s and we let $x \rightarrow X$ on the right hand side. The solution $X(Z)$ is, in a sense, generic (except for the specification of τ_r in $\Phi(Z)$), because the function $X(Z)$ is fitted to an orthogonal coordinate system in which Z is one of the two coordinates. The coordinate system is defined as the $(\chi - Z)$ system, in which we write $\chi = X(Z)$ to define the flame shape. The furthest upstream point of the PF arc occurs at $\chi = 0$, so that the distance between the origin and the line $\chi = 0$ is given by X_0 . When lines of constant (χ, Z) form an orthogonal grid, lines of constant χ can be deduced from lines of constant Z through the equation:

$$\nabla \chi \cdot \nabla Z = 0, \quad (5)$$

which is written in a scalar notation as

$$\chi_x Z_x + \chi_y Z_y = 0.$$

The boundary values of χ are obtained from the requirement that they remain unchanged regardless of the value of ε , so our solutions for the boundary values of χ can be developed analytically from the $\varepsilon = 0$ case for the convective flow cases. The χ -equation is a two

dimensional wave equation with variable coefficients. The only difficulty is that the “wave speed”, $c = Z_x/Z_y$, shows a very strong variation near the singular point of $Z(x,y)$ at the origin (ranges from $-\infty$ to $+\infty$ across the origin in the y -direction). This difficulty is eliminated by halving the domain and imposing symmetry requirements across the x -axis. The solution is obtained using a finite differencing scheme incorporating an unsymmetric algorithm, as suggested by Pearce and Mitchell [1962].

The substitution of Eq.(2.5) for s with Eq. (2.8) for $\Phi(Z)$ and Eq. for $\hat{T}_0(Z)$ produces a nonlinear ODE for $X(Z)$. Note that we must use $x \rightarrow X_0 + X$ on the right hand side of Eq. (5). The solution of this ODE produces two **PF** arcs, one for $s > 0$, reaching toward the fuel side, and one for $s < 0$ reaching toward the oxidizer side. These flame shapes can be compared with the numerical solutions of the original equations.

There is an important obstacle to the completion of this task. This arises in Eq.(2.8), through the value of Φ evaluated at Z_f (the flame tip), where the **DF** and the two

PFs meet. Here we obtain the following relationship, $\Phi(Z_f) = \left(4 \frac{(1 - Z_f)}{\kappa^2}\right) \cdot \left(\frac{Dr_q^2}{\beta^3}\right)$.

When this quantity is less than unity Eq.(2.5) produces two distinct and opposite **PF** slopes leaving the triple point. When $\Phi(Z_f) > 1$, Eq.(2.5) gives imaginary slopes, so the **PFs** do not emanate from the triple point. Both of these physically unrealistic choices can be avoided by requiring through the choice of κ as

$$\kappa = \left[(1 - Z_f) \left(\frac{Dr^2}{\beta^3} \right) \right]^{\frac{1}{2}}, \quad (6)$$

which has the added benefit of fixing the temperature gradient $\tau_r = \frac{\kappa}{r_q}$ upstream of the PF

arc. Our analysis, as already discussed, requires $\kappa > 1$. Eq.(2.8) reduces to

$$\Phi(Z) = \left(1 + \frac{\gamma}{2} \right) \left[\frac{\hat{T}_0(Z)}{\hat{T}_f} \right]^6 \exp \left(\frac{\hat{E}}{\hat{R}} \left(\frac{1}{\hat{T}_o(Z)} - \frac{1}{\hat{T}_f} \right) \right). \quad (28)$$

Another obstacle in our quest for the solution for the flame shapes is the absence from our theory of X_0 . As a consequence, we determine X_0 from the numerical solution and employ it as an empirical “input” parameter. This obstacle enables us to compute our solution for dX/dZ from Eqs. (2.5), (4), (2.7), (2.9) and (2.10) with the result the **PF** arcs shapes $\chi=X(Z)$, are obtained that can be compared with numerical predictions.

CHAPTER 4

RESULTS AND DISCUSSION

Shown in Fig. 7 is a sample test plot of the **PF** arcs superposed onto the physical coordinate system. The solution for the **PF** Arcs on the oxidizer side and the diffuser side are obtained by solving the inner problem through a finite differencing scheme. The problem has to be numerically integrated from the triple point towards both the oxidizer side and the fuel side of the trailing diffusion flame.

Once this solution is obtained, the field equations for Z are solved through a *successive over relaxation (SOR) method*. The solution at this stage is fairly straightforward. Then in order to graft the solution onto the physical coordinate system, we have to determine the solution for the set of contours which are orthogonal to the Z -field at every point. This is achieved in two stages. First the case for no convection, $\epsilon=0$, is solved analytically using conformal transformations. Then this solution is evaluated at the boundaries for use as an “*initial*” value for the corresponding non-zero convection field equation; the resulting wave equation has to be solved in order to find the orthogonal χ - Z

coordinate grids for various convective inflows (see Fig. 12).

However, the solution to this problem is not trivial, since the “wave speed” given by the ratio of dZ/dy and dZ/dx shows strange behavior at the singular origin in the y -direction. This is because of the fact that although dZ/dx shows no sign change across the entire domain of interest, dZ/dy passes through a sign change at the triple point, **TP**. As a result the entire term undergoes this sign change and the result is numerically devastating (refer to Figs. 14 and 15). This problem can be circumvented by halving the domain and imposing symmetry requirements across the x -axis. Once this is accomplished a combination of unsymmetric algorithms as suggested by Pearce and Mitchell [1962], is used to solve the problem.

Shown in Figs. 8 through 11 are comparisons of the asymptotically-calculated flame shapes with the reactivity contours of the numerical model. The congruence of these curves is quite good, given the many approximations suffered in the theoretical calculation. There are, nevertheless, a few subtle points worth mentioning.

First, the theoretical solution was grafted onto the arc $Z=Z_f$. The reactivity maximum from the numerical computations was therefore shifted, (in practice, only very slightly) to the line $Z = Z_f$, and this point (X_0, Z_f) was taken as the origin for the flame shape calculations.

Second, the χ -Z grid is generally calculated for the case $\epsilon > 0$, indicating a non-zero convective flow. However in our derivation of dX/dZ we passed to the limit $\epsilon = 0$ for simplicity and generality (because our analytical solution was valid only near $Z_f = 1/2$). *How can an analytical solution obtained in the limit $\epsilon = 0$ be grafted onto a grid calculated for $\epsilon > 0$?* The answer to this question in fact provides another check on the validity of our solution. It is not difficult to demonstrate that when ϵ increases, the **PF** arc should become progressively more gently bowed. Physically, this indicates that the convective delivery of reactants to the **PF** arcs strengthens them, enabling them to “face” the oncoming flow more squarely. Consequently, for the limit $\epsilon \rightarrow 0$, the sweepback of the **PF** arcs should be a *maximum*. We see from the figures that our theoretically calculated **PF** arcs are always swept back further than the numerically-calculated **PF** arcs. This, in our view, is a rather strong endorsement of the validity of our approach. In other words, the relative degrees of sweepback are *qualitatively as they should be*. We note, parenthetically, that the differences between the χ and Z contours for $\epsilon = 0$ and $\epsilon > 0$ are significant only in a region between the walls and the far-downstream region. The differences, even in the intermediate region, are not large.

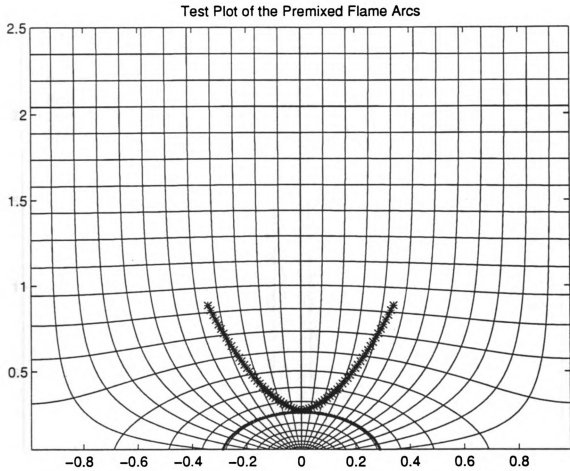


Fig 7. Sample test plot of the PF arcs.

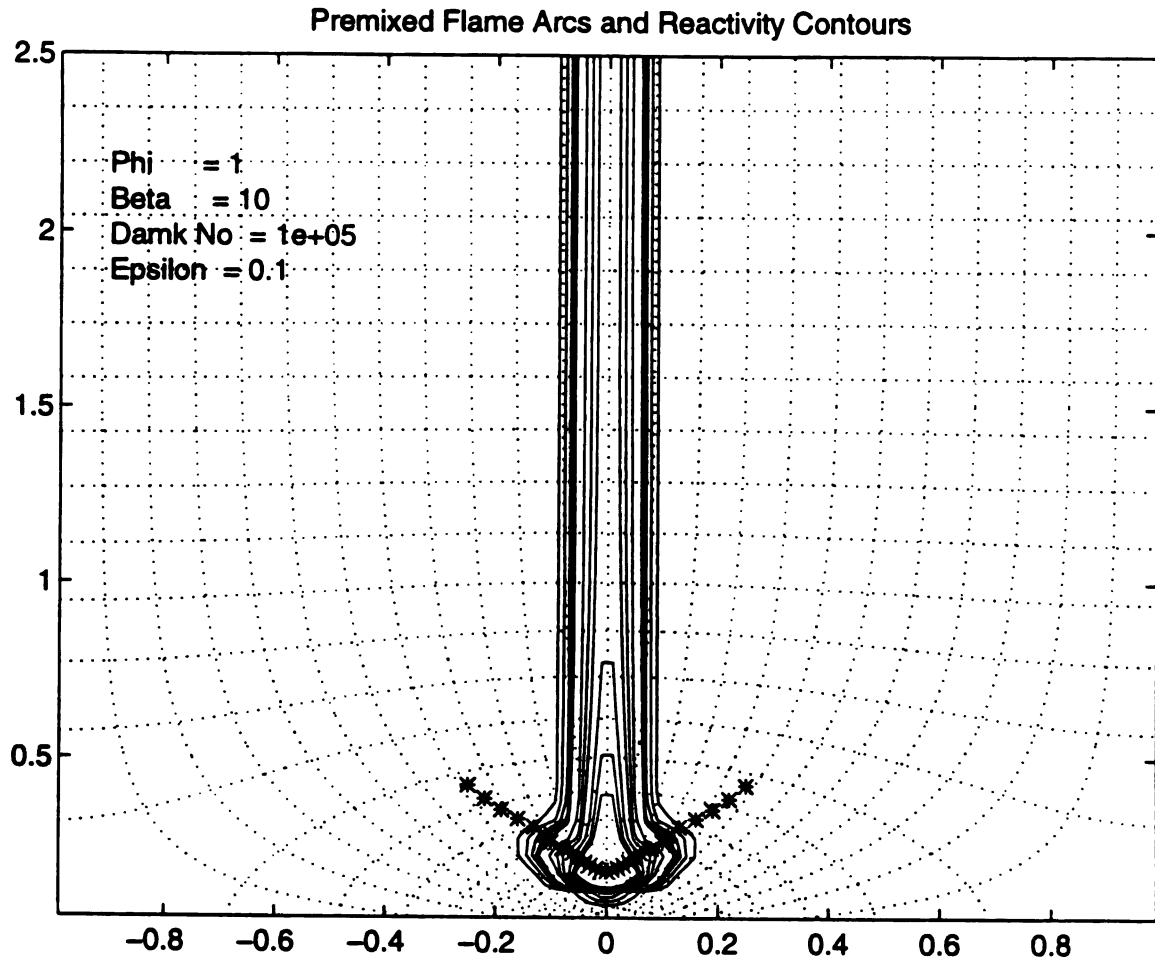


Fig 8. Premixed flame arcs superposed onto the orthogonal coordinate system. The reactivity contours are also plotted for the same case.

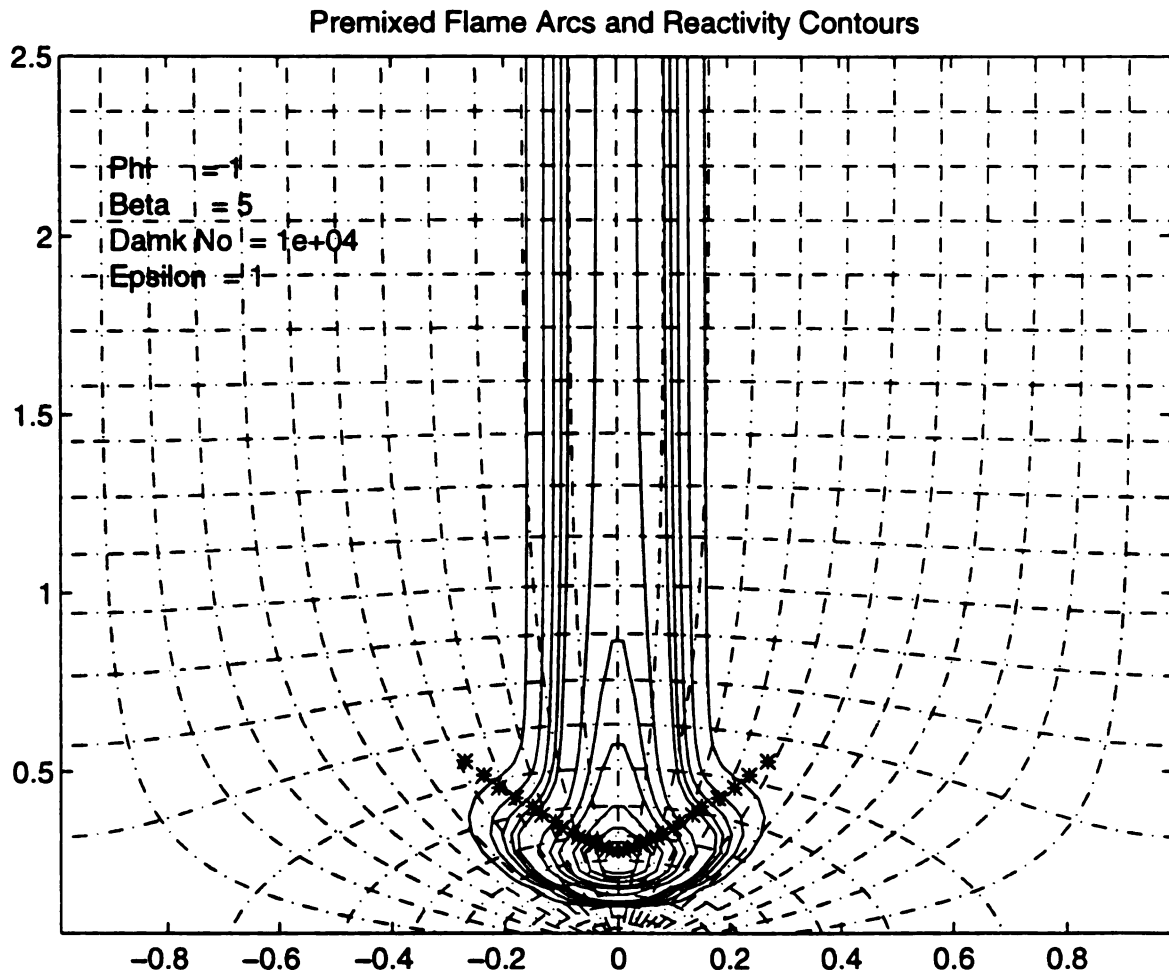


Fig 9. Premixed flame arcs superposed onto the orthogonal coordinate system. The reactivity contours are also plotted for the same case.

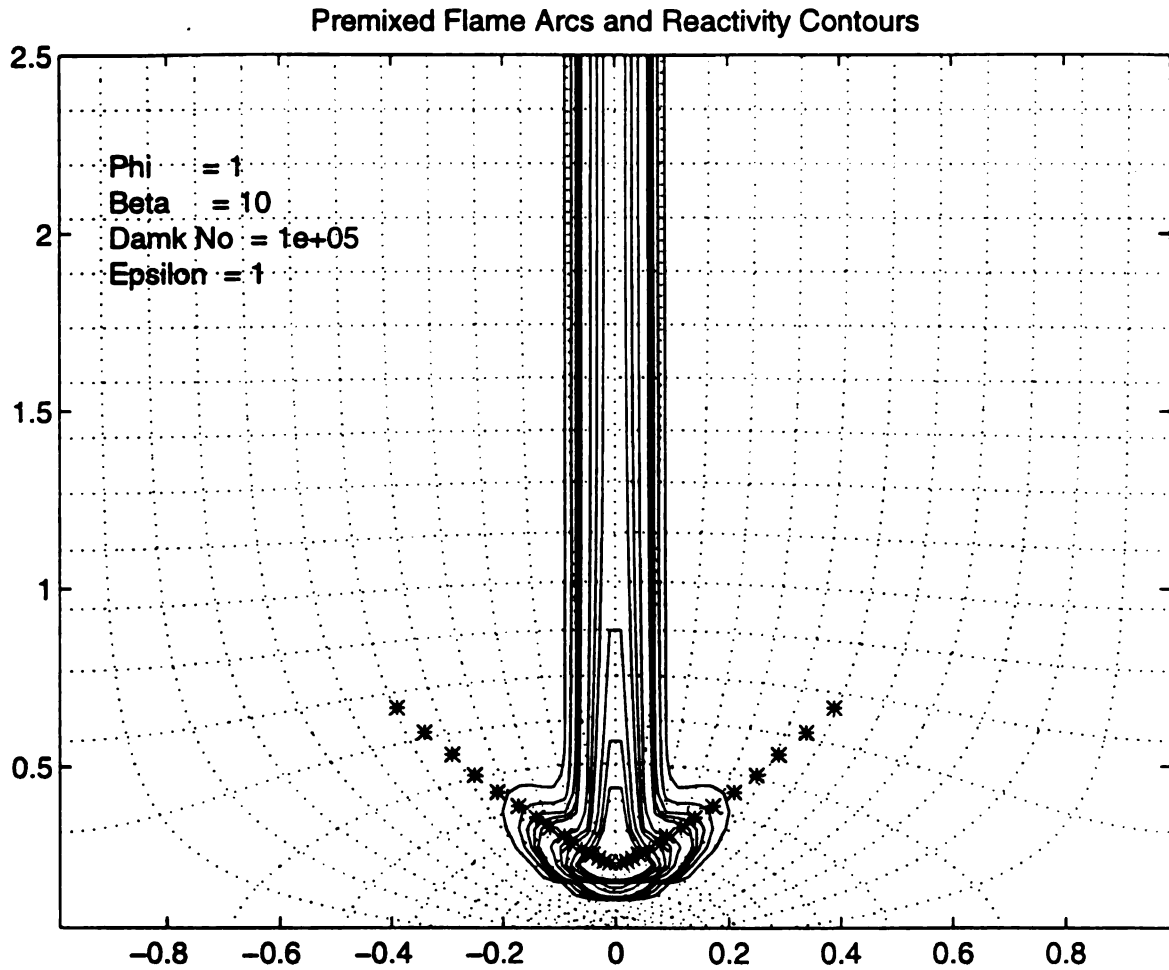


Fig 10. Premixed flame arcs superposed onto the orthogonal coordinate system. The reactivity contours are also plotted for the same case.

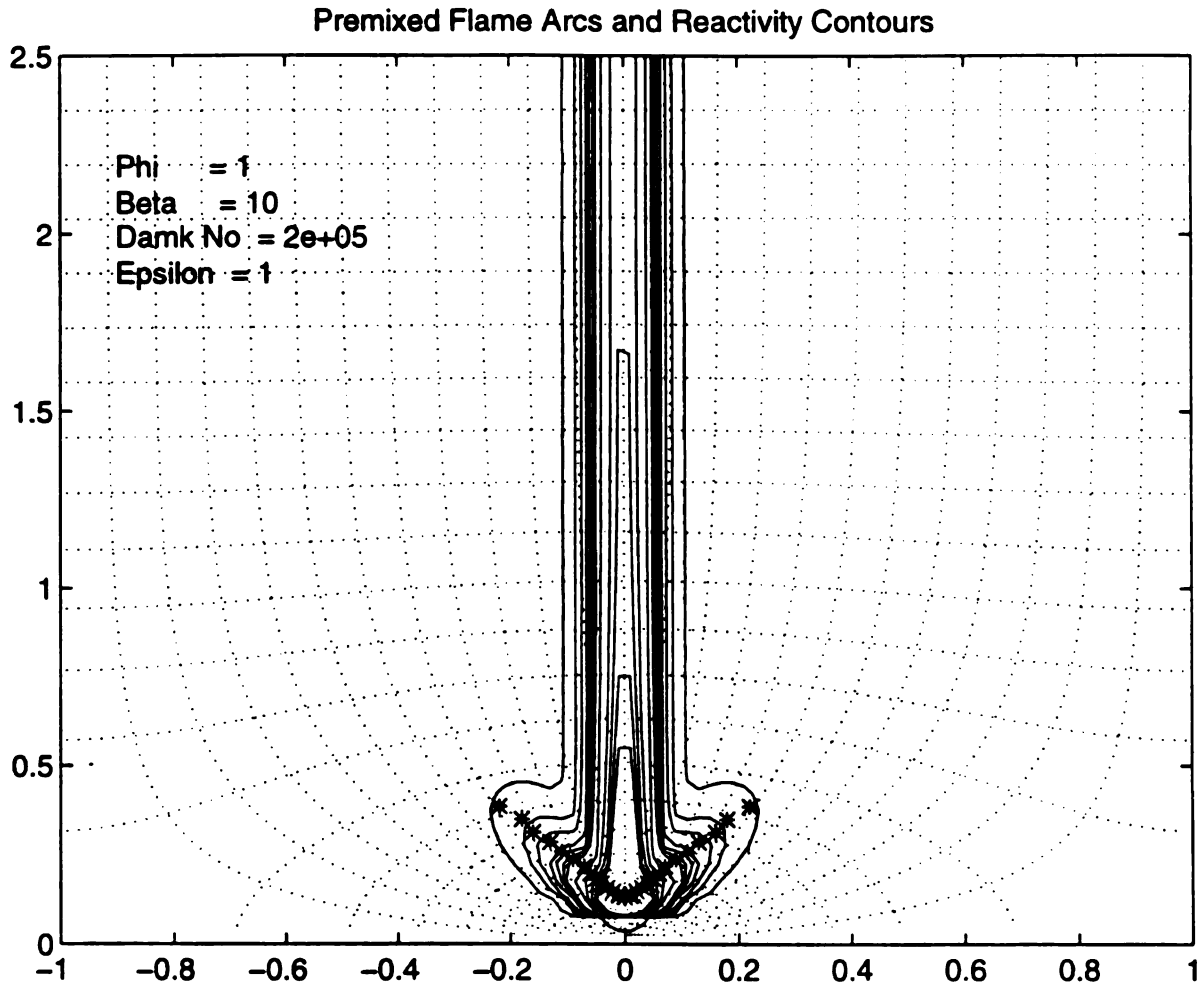


Fig 11. Premixed flame arcs superposed onto the orthogonal coordinate system. The reactivity contours are also plotted for the same case.

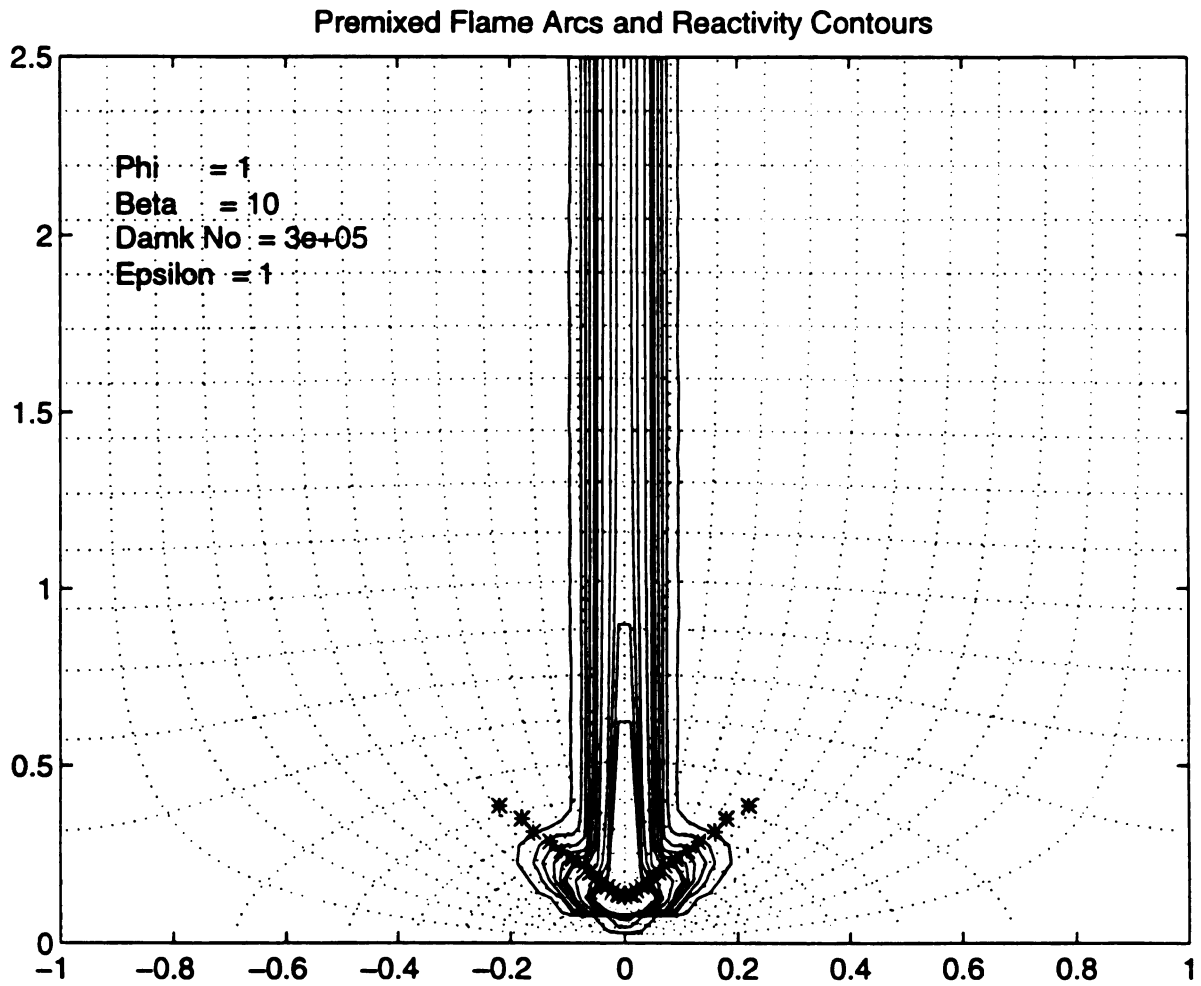


Fig 12. Premixed flame arcs superposed onto the orthogonal coordinate system. The reactivity contours are also plotted for the same case.

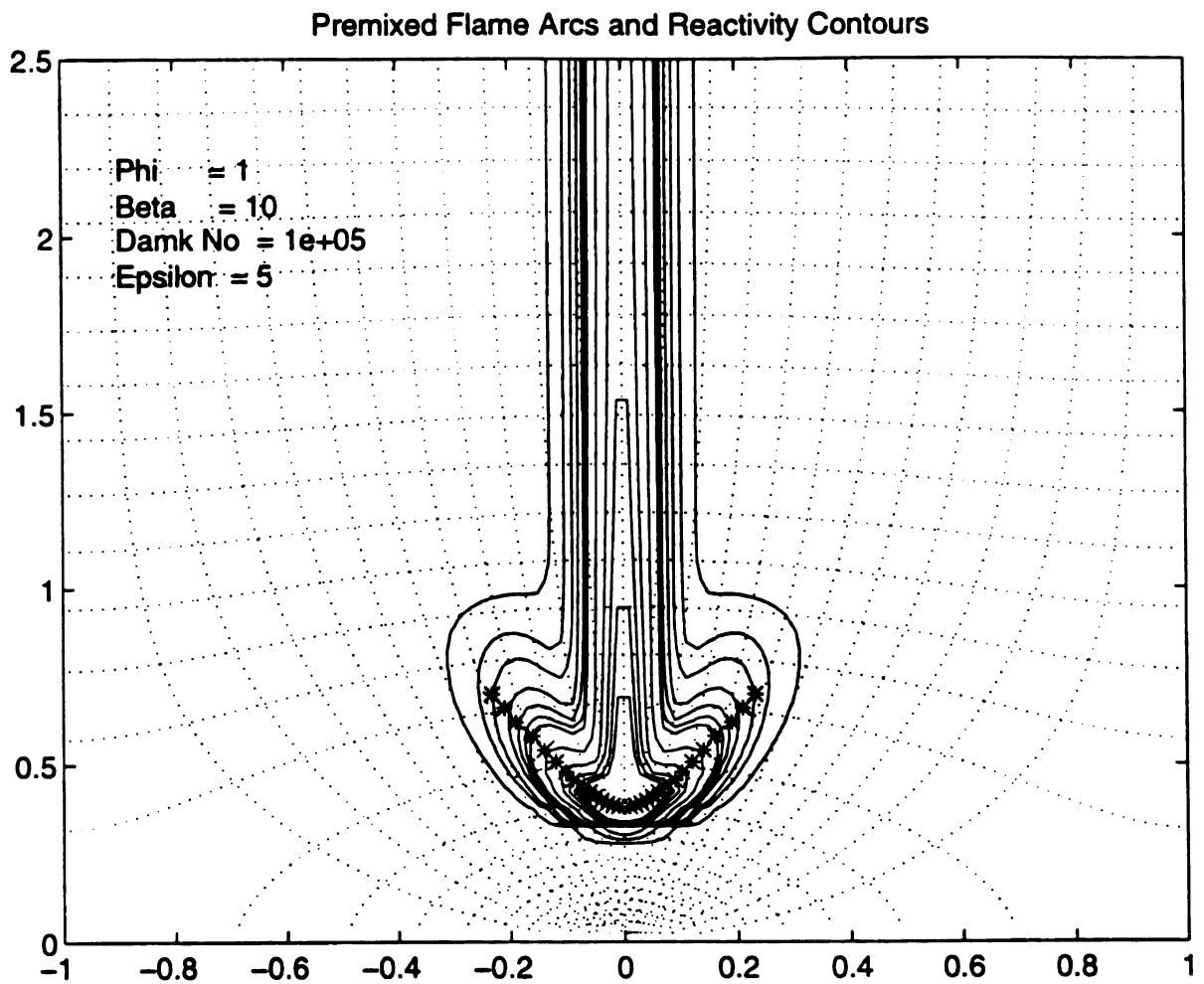


Fig 13. Premixed flame arcs superposed onto the orthogonal coordinate system. The reactivity contours are also plotted for the same case.

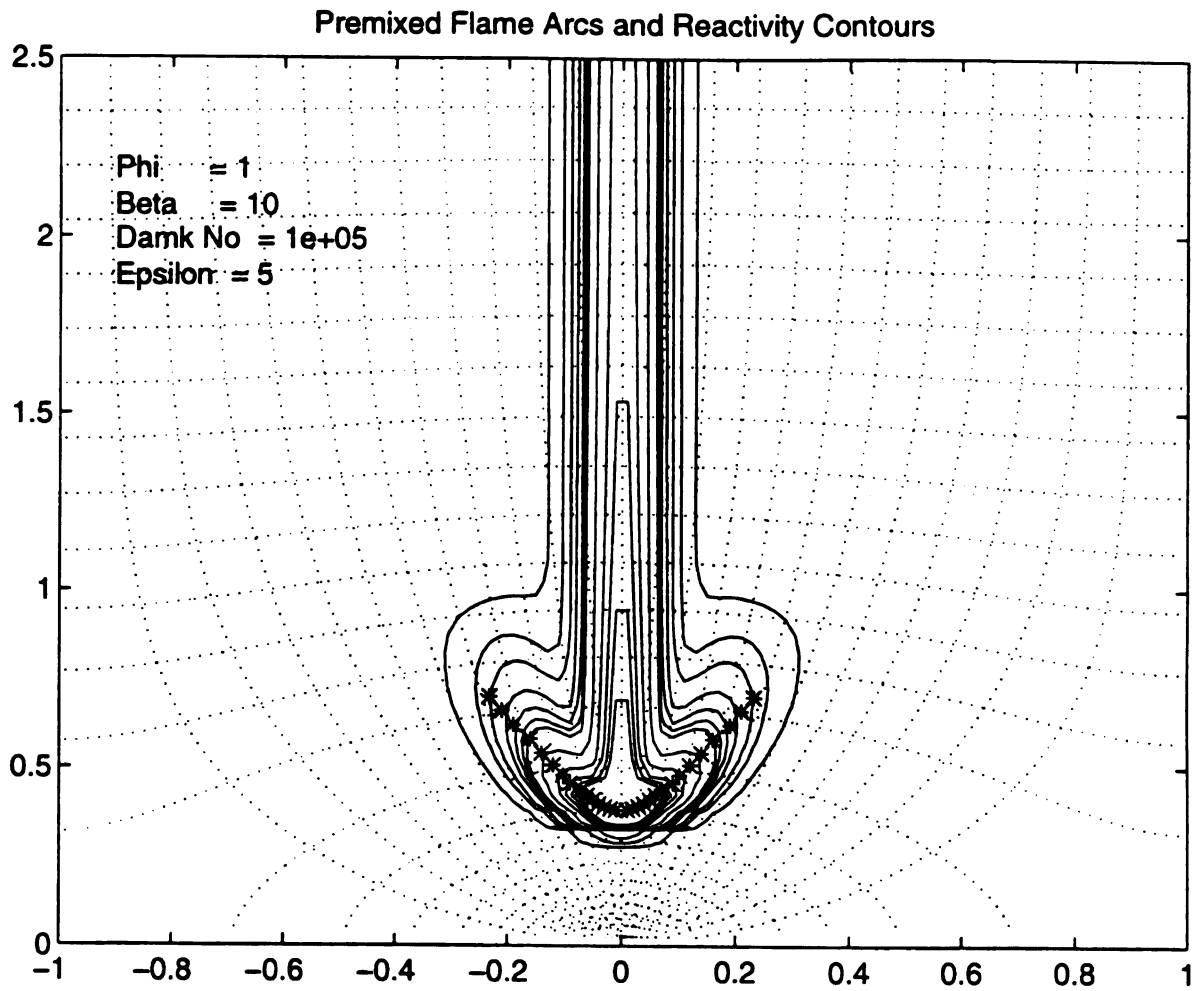


Fig 13. Premixed flame arcs superposed onto the orthogonal coordinate system. The reactivity contours are also plotted for the same case.

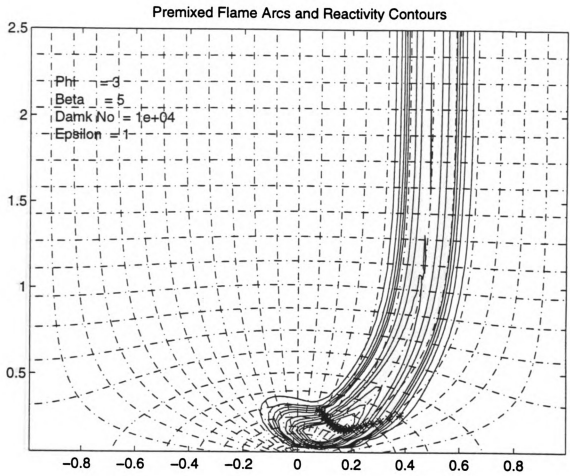


Fig 14. Premixed flame arcs superposed onto the orthogonal coordinate system. The reactivity contours are also plotted for the same case.

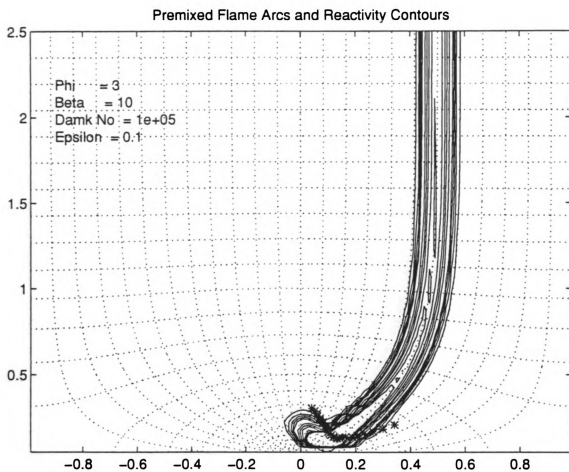


Fig 15. Premixed flame arcs superposed onto the orthogonal coordinate system. The reactivity contours are also plotted for the same case.

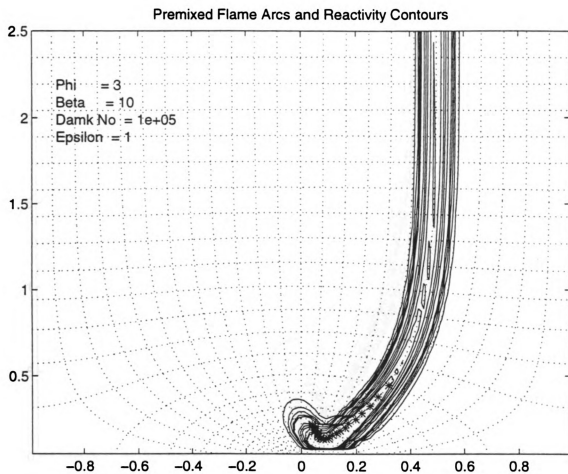


Fig 16. Premixed flame arcs superposed onto the orthogonal coordinate system. The reactivity contours are also plotted for the same case.

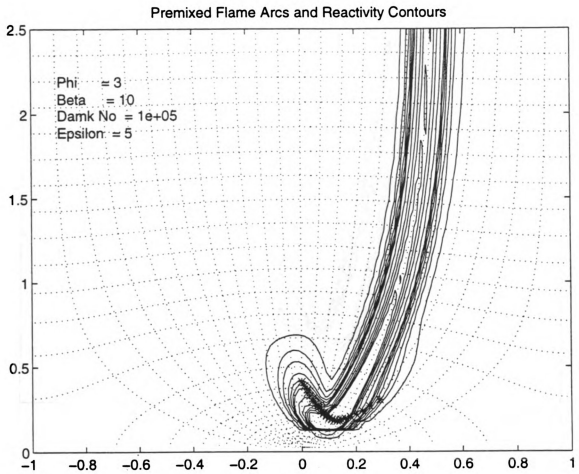


Fig 17. Premixed flame arcs superposed onto the orthogonal coordinate system. The reactivity contours are also plotted for the same case.

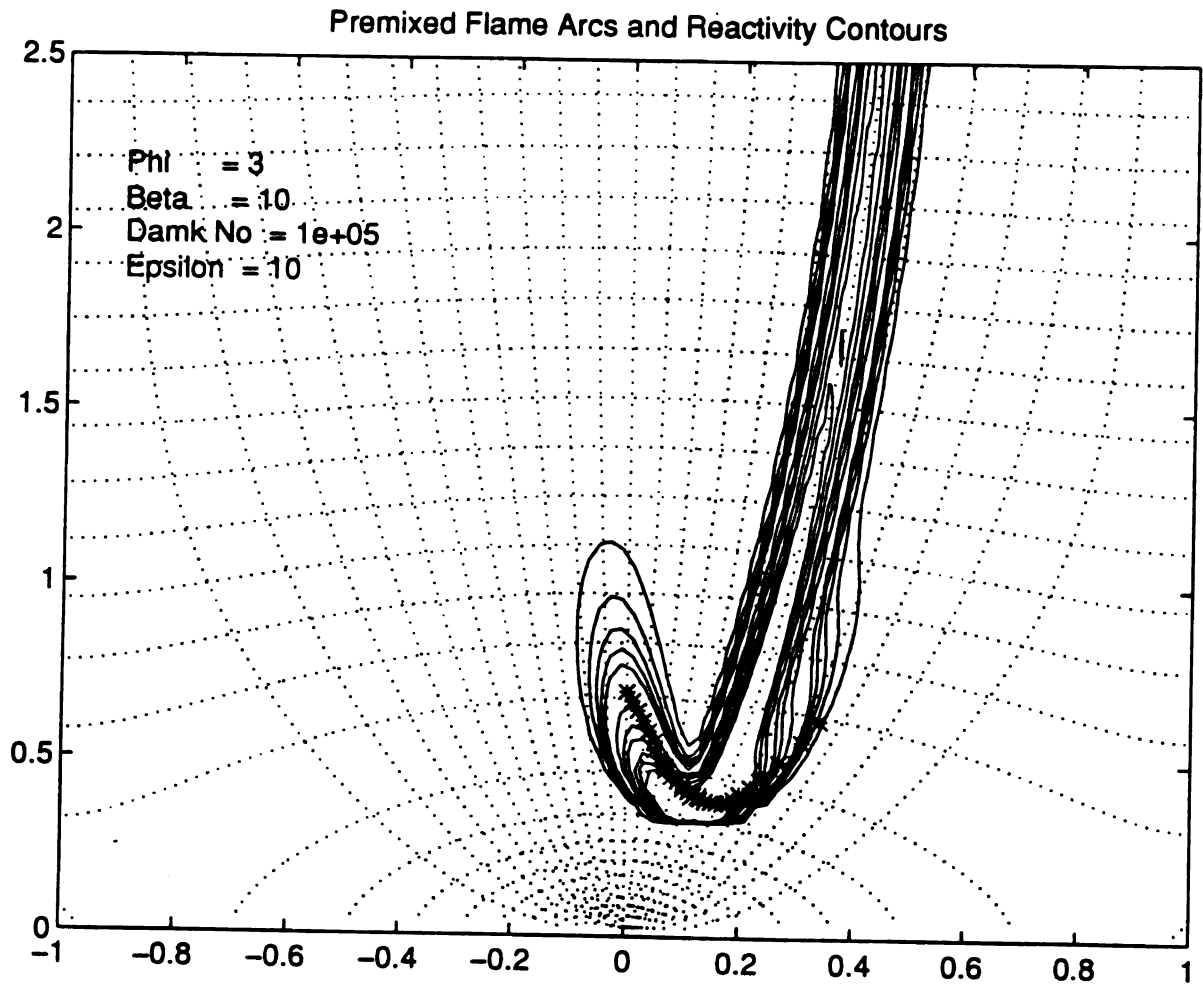


Fig 18. Premixed flame arcs superposed onto the orthogonal coordinate system. The reactivity contours are also plotted for the same case.

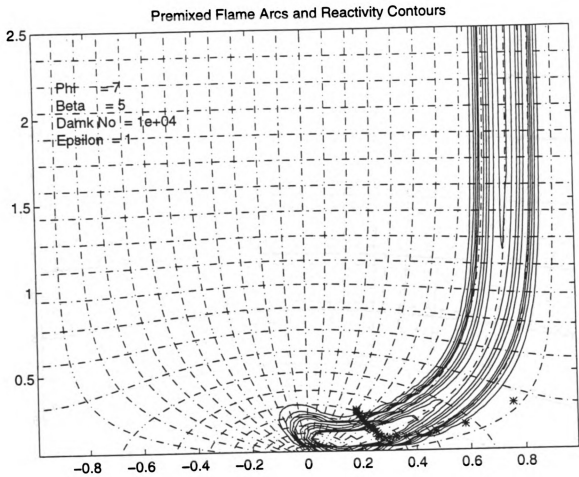


Fig 19. Premixed flame arcs superposed onto the orthogonal coordinate system. The reactivity contours are also plotted for the same case.

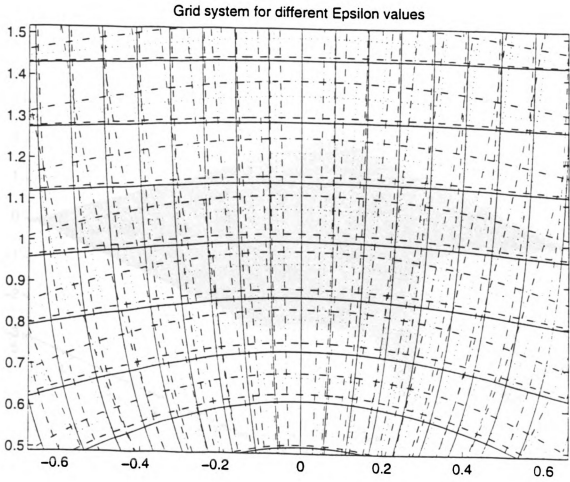


Fig 20. Grid system for different epsilon values.

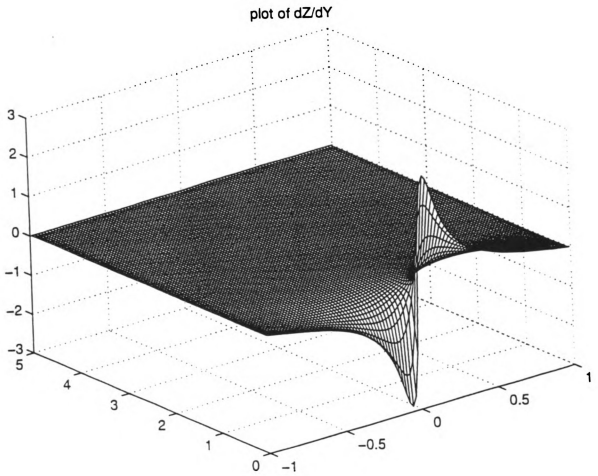


Fig 21. Plot of dZ/dY for the domain.

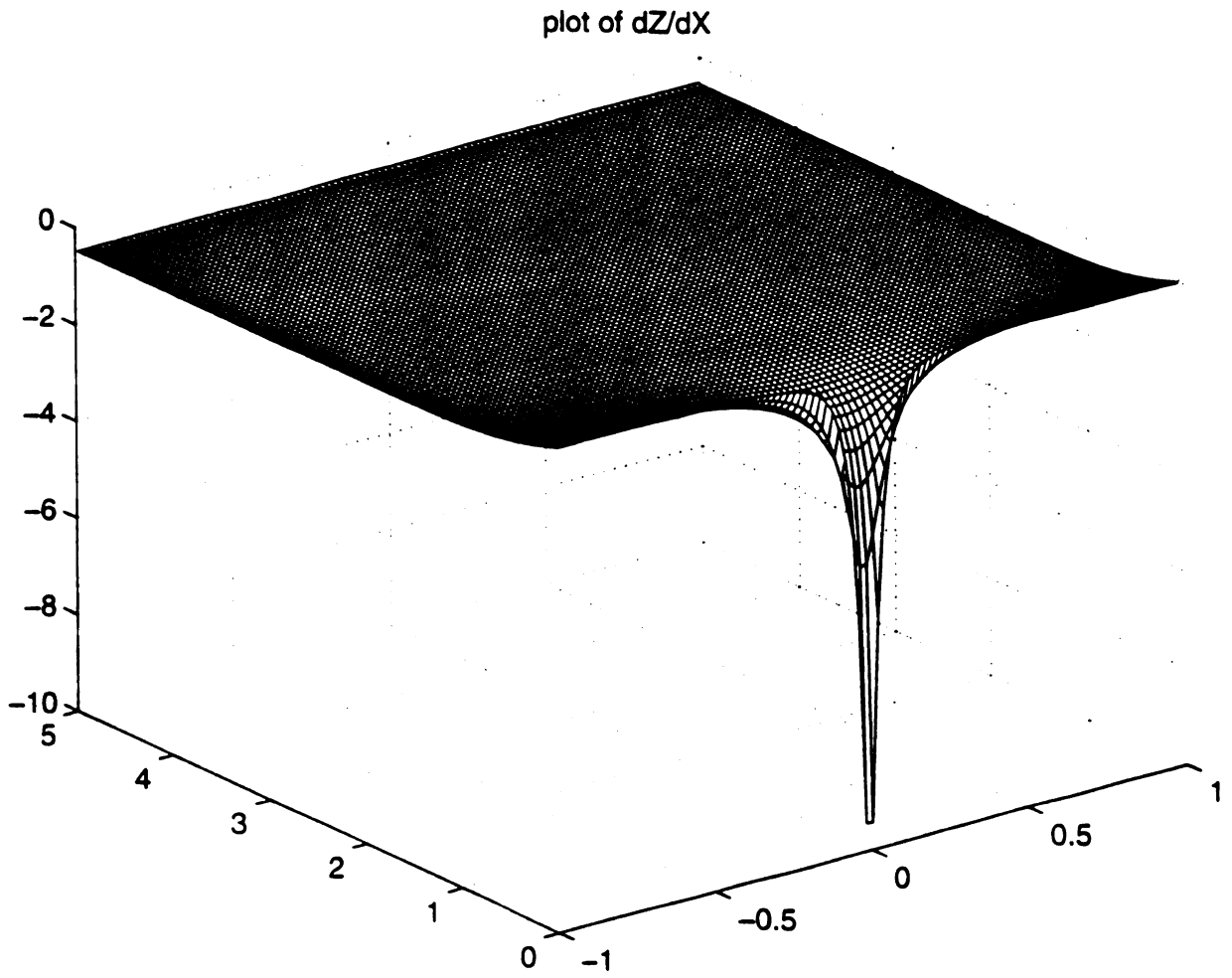


Fig 22. Plot of dZ/dX for the domain.

CHAPTER 5

CONCLUSIONS AND RECOMMENDATIONS

FOR FUTURE WORK

We have demonstrated that a fairly simple theoretical approach successfully predicts the **PF** arc shape near the triple point (**TP**), where the flame attaches to the cold surface. The flame arc near the triple point is rounded, contrary to the discussion of Wichman [1995], where it was shown that non-isenthalpic **PF** arcs may demonstrate an arrow-like or pointed flame structure. However, the derivations of Wichman [1995] considered $\beta \rightarrow \infty$, which eliminated the inner region, for which careful scrutiny will always generate continuous solutions. In fact, our basic premise, $\Phi(Z_f) = 1$, follows directly from the philosophic requirement that discontinuities cannot be tolerated at the smallest scales. This premise is of course interchangeable with the continuum hypothesis.

A challenge greater than the calculation of the flame shapes is the calculation of quenching distances [Wichman (1989)]. Once this is achieved, it will no longer be necessary to treat (X_0, Z_f) as “input parameters”. Rather, X_0 shall be estimated from an asymptotic analysis and used in a theory like the one described here.

There are still numerous weak points in this work that future studies should examine. The first is the use of the simplistic Burke-Schumann profile for the *upstream* (quenching region) temperature field. In reality, no more than the *downstream* cross-**DF** temperature field should be used. When this is attempted, we find that the location of maximum Φ , defined as $Z_{\Phi_{\max}}$, shifts (toward a larger Z when $Z_f < 1/2$) and that a slope discontinuity develops at Z_f , rendering the Φ -profile between Z_f and $Z_{\Phi_{\max}}$ slightly unrealistic. A smoothening or “renormalization” procedure has been developed to cope with this difficulty, but further analysis has to be carried out before it can be incorporated into the final solution. In the general case, the outer solution must of course be obtained numerically through the solution of elliptic partial differential equations that are coupled through a boundary condition to the inner (flame) zone. A general solution procedure utilizing numerical matching is now being developed.

BIBLIOGRAPHY

BIBLIOGRAPHY

Dold, J.W., "Flame Propagation in a Non-Uniform Mixture: Analysis of a Slowly Varying Triple Flame", Comb. and Flame, 76, pp. 71-88 (1989)

Linan, A., "The Asymptotic Structure of Counter Flow Diffusion Flames for Large Activation Energies", Acta Astronautica, 1 1007 (1974)

Pearce, R.P, and Mitchell, A.R., Math. Comput., 16, 155, 1962.

Wichman, I.S., "On the Quenching of a Diffusion Flame near a Cold Wall", Comb. Sci. and Tech. (1989)

Wichman, I.S., "The Basic Features of Triple Flames in Combustion Theory", 8th ISTP meeting, San Francisco, CA (1995)

Wichman, I.S., and Bruneaux, G., "Head-On Quenching of a Premixed Flame by a Cold Wall", accepted for publication in Comb. and Flame. To appear (1996)

MICHIGAN STATE UNIV. LIBRARIES



31293014051910